

Submitted to Physical Review D

The Effects of Correlations on Neutrino Opacities in Nuclear Matter

Adam Burrows

Department of Astronomy, The University of Arizona, Tucson, AZ 85721
e-mail: burrows@as.arizona.edu

R. F. Sawyer

Department of Physics, The University of California, Santa Barbara, CA 93106
e-mail: sawyer@sarek.physics.ucsb.edu

Abstract

Including nucleon–nucleon correlations due to both Fermi statistics and nuclear forces, we have developed a general formalism for calculating the neutral–current neutrino–nucleon scattering rates in nuclear matter. We derive corrections to the dynamic structure factors due to both density and spin correlations and find that neutrino–nucleon scattering rates are suppressed by large factors around and above nuclear density. Hence, in particular for the ν_μ and ν_τ neutrinos, but also for the ν_e neutrinos, supernova cores are more “transparent” than previously thought. The many–body corrections increase with density, decrease with temperature, and are roughly independent of incident neutrino energy.

In addition, we find that the spectrum of energy transfers in neutrino scattering is considerably broadened by the interactions in the medium. An identifiable component of this broadening comes from the absorption and emission of quanta of collective modes akin to the Gamow–Teller and Giant Dipole resonances in nuclei (zero–sound; spin sound), with Čerenkov kinematics.

Under the assumption that both the charged–current and the neutral–current cross sections are decreased by many–body effects, we calculate a set of ad hoc protoneutron star cooling models to gauge the potential importance of the new opacities to the supernova itself. While the early luminosities are not altered, the luminosities after many hundreds of milliseconds to seconds can be increased by factors that range from 10% to 100%. Such enhancements may have a bearing on the efficacy of the neutrino–driven supernova mechanism, the delay to explosion, the energy of the explosion, and the strength and relative role of convective overturn at late times. However, the actual conse-

arXiv:astro-ph/9801082v1 11 Jan 1998

quences, if any, of these new neutrino opacities remain to be determined.

I. INTRODUCTION

In core-collapse supernovae, neutrinos are arguably the engines of explosion [1–5] and the best direct probe of its internal workings [6–9]. To understand the supernova phenomenon, a theorist requires knowledge of the equation of state of nuclear matter, stellar evolution, general relativity, statistical physics, and the techniques of radiative transfer and hydrodynamics. However, the opacities and sources of neutrinos of all the six known neutrino species take center stage in this context in which the neutrino “optical” depth down to the protoneutron star core varies from 10^3 to 10^6 , neutrino luminosities can approach 10^{54} ergs s^{-1} , and photons, the traditional agents of radiative energy transfer in astrophysics, are profoundly trapped. This seems to be a unique role for neutrinos in the universe. Since neutrinos are abundantly produced, yet are the most mobile of a collapsed core’s constituents, their microphysics determines the outcome of core collapse, neutron star and black hole formation, nucleosynthesis at and beyond the iron peak [10,11], early pulsar kinematics [12], and, perhaps, the asymmetries observed in supernova debris clouds [13].

In the neutrino-driven mechanism, neutrinos liberated from the core heat matter in the inner stellar envelope (the outer protoneutron star envelope) as they emerge. If the total heating rate is sufficient, the envelope becomes unstable and is ejected. It has recently been shown [2–4,14] that neutrino-driven convection in this inner mantle can make this process more efficient (but see [15]). Hence, neutrinos mediate the energy transfer from the core to the mantle and their luminosities and spectra are crucial to the viability and character of the explosion mechanism. These in turn are a function of the neutrino-matter opacities.

While at low mass densities ($\rho < 10^{12}$ gm cm^{-3}) neutrino-matter cross sections are well-understood and characterized [16–18,26], at the higher densities achieved in core collapse the inter-particle spacings are smaller than the wavelength of the ambient neutrinos and many-body effects and particle-particle correlations must be taken into account. Ion-ion correlations due to Coulomb interactions have been addressed in the supernova context (*cf.* [19]) and their effects, though interesting, have been shown to be small and transient [20]. However, near and above nuclear densities ($\sim 2.6 \times 10^{14}$ gm cm^{-3}) neutrinos with energies below ~ 1000 MeV “see” many nucleons and collective effects must be considered. In fact, these effects can radically alter the opacity of nuclear matter to neutrinos, since the nuclear force introduces strong correlations near and above nuclear densities.

Many-body effects have been discussed before in the protoneutron star and supernova context (*cf.*, [21–25]), but the results were either too approximate or of too-limited scope. Pauli blocking by final-state nucleons, a type of correlation, has been a component of supernova and protoneutron star thinking for some time [9,26,27], but the approximate treatments employed at high densities can be off by large factors (§VI.B). Furthermore, in the case of neutrino-nucleon scattering, the assumption that the scattering is elastic [28] and that the nucleons are stationary can be shown to result in errors in the energy transfer of as much as a factor of ten. A consequence of this is that energy equilibration of ν_μ and ν_τ neutrinos is brought about not by the $\nu + \bar{\nu} \rightarrow e^+ + e^-$ process or neutrino-electron scattering, but by neutrino-nucleon scattering. This result, one by-product of this study, has also been found by Hannestad & Raffelt [29] and in the pioneering work of Reddy *et al.* [30]. The latter have conducted the most complete exploration of high-density neutrino opacities to date, taking care to calculate them in a manner consistent with a reasonable nuclear equation of

state (see also [31,32]). Some of our results and formalism recapitulate theirs. However, Reddy *et al.* [30] neglected particle–particle and spin–spin correlations and focussed on the kinematic effects of nuclear interactions. We find that the effect of many–body correlations on neutrino–matter cross sections can be quite large. Nuclear matter is more “transparent” to neutrinos than we had heretofore imagined.

Neutrinos interact with nucleons via both charged–current and neutral–current processes. The charged–current processes predominate for the electron-type neutrinos by a few factors, while the neutral current predominates for ν_μ and ν_τ neutrinos. The latter carry away more than 50% of the binding energy of the neutron star. We have found that at the high densities achieved in collapse, both the charged–current and the neutral–current cross sections are dramatically affected by nuclear correlation effects. In this paper, we focus on neutral–current neutrino–nucleon scattering, both the Fermi and the Gamow–Teller parts, and defer a discussion of the charged–current many–body effects to a later paper. Our formalism is good for any degree of nucleon degeneracy and fully incorporates the effects of reaction kinetics, Pauli blocking, and correlations due to interactions. Energy transfers both to and from the nucleons are consistently included. One product of this paper is a formalism for calculating in full the dynamic structure functions for neutrino–nucleon processes.

The effect of increased transparency at high densities on the neutrino–driven mechanism of core–collapse supernovae is not yet clear. Supernova theory is notorious for its mitigating feedbacks and false leads. The early ($\lesssim 500$ milliseconds) neutrino luminosities and spectra depend upon the material in the outer shocked mantle of the protoneutron star, where we think we understand neutrino cross sections. As a consequence, we don’t expect that our understanding of this early phase will be altered by the new opacities. Even if it could be shown that neutrino cross sections at the lower densities around the neutrinospheres and near the shock were in some non–trivial sense different, increased transparency would lead to an increased rate of collapse of the mantle, which, in turn, would lead to higher densities, which would partially quench the effect. The corrections to the scattering rates we address in this paper are more relevant at later times ($> 500 - 2000$ milliseconds), for it is then that the emergent luminosities are powered by the energy in the dense core. At this time, since most of the core pressure is derived from the cold, stiff nuclear component, and not an ideal gas of non–interacting nucleons, the effective specific heat is not negative, but positive, and cooling does not lead to much of a density change. Therefore, the effect of a decrease in opacity will not be partially cancelled by a density increase and the emergent luminosities will reflect the full suppression effects. Since the neutrino luminosity is the agency of explosion, this could be important for a model in which the delay to explosion is not short. There is an important caveat: accretion of the infalling envelope is a major power source and its continuance can mask the effects of the alterations we find in the neutrino opacities at depth. Accretion will be less important for the lower–mass progenitor stars ($8 - 13 M_\odot$), which have more tenuous envelopes. In addition, the neutrino signals observed from SN1987A [6,7] constrain the magnitude of any alteration in our standard model, as does the fact that there is a fixed amount of energy to be radiated from any given protoneutron star. In this paper, to gauge these effects and to begin the debate on these issues, we perform an idealized protoneutron star cooling calculation.

In §II, we explain the physics of the correlation effects and provide a simple, single–channel, model that makes clear the character of the results. In §III, the general formulation

is presented, as is an aside on the low-wavelength limit. In §IV, the complete correlation and dynamic structure function formalism is derived and discussed and a straightforward nucleon potential model is described. In reality, the solution of the problem of the nuclear equation of state goes hand-in-hand with the calculation of many-body correlations. Since we are not proposing here to resolve the former, we are satisfied with a model that captures the essence of the nuclear interaction. Different nuclear equations of state will yield quantitatively, but not qualitatively, different results. In §V, we outline our multi-channel formalism for calculating ν -nucleon scattering structure functions and in §VI we present the results of our calculations for various temperatures, densities, and neutrino energies. In §II through §VI, we start from the general expressions of statistical mechanics that encompass the effects of the medium on the neutral-current neutrino reactions and proceed to calculations of the effects. In §VII, we present the results of a suggestive series of calculations that might point to the astrophysical import of the new effects and in §VIII we summarize our conclusions.

II. THE ESSENTIAL PHYSICS

We can introduce, and qualitatively explain, much of what is to come in a simplified system in which we have just one species of non-relativistic nucleon with mass m , which is coupled to neutrinos through only a vector neutral current. We take the weak-interaction Lagrangean density to be,

$$\mathcal{L}_W = \frac{G_W}{\sqrt{2}} \bar{\psi}_\nu(x) (1 - \gamma_5) \gamma_0 \psi_\nu(x) n(x), \quad (1)$$

where $n(x)$ is the density operator for the nucleons, G_W is the weak coupling constant, and the other symbols have their standard field-theoretic meanings. In the following, we employ a system of units in which $\hbar = c = k_B = 1$.

We write the differential rate of neutrino scattering $\mathbf{p}_1 \rightarrow \mathbf{p}_2$ in the medium as

$$\frac{d^2\Gamma}{d\omega d\cos\theta} = (4\pi^2)^{-1} G_W^2 (E_1 - \omega)^2 [1 - f_\nu(E_1 - \omega)] \Lambda^{00}(q, \omega) S(q, \omega), \quad (2)$$

where f_ν is the occupation function for neutrinos, E_1 is the energy of the incident neutrino, Λ is the neutrino trace,

$$\Lambda^{\mu\nu} = (4E_1E_2)^{-1} Tr[\not{p}_1 (1 - \gamma_5) \gamma^\mu \not{p}_2 \gamma^\nu (1 - \gamma_5)], \quad (3)$$

ω is the energy transfer ($|\mathbf{p}_1| - |\mathbf{p}_2|$) to the medium, and q is the momentum transfer ($|\mathbf{p}_1 - \mathbf{p}_2|$), related to ω and p_1 through the neutrino scattering angle, θ , by

$$q = [p_1^2 + (p_1 - \omega)^2 - 2p_1(p_1 - \omega) \cos\theta]^{1/2}. \quad (4)$$

For the case of free nucleons, the nucleon part, $S(q, \omega)$ (the *dynamic* structure function) is given by

$$S(q, \omega) = 2 \int \frac{d^3p}{(2\pi)^3} f(|\mathbf{p}|) (1 - f(|\mathbf{p} + \mathbf{q}|)) 2\pi \delta(\omega + \epsilon_{\mathbf{p}} - \epsilon_{\mathbf{p}+\mathbf{q}}), \quad (5)$$

where $f(|\mathbf{p}|)$ is the Fermi–Dirac distribution function and $\epsilon_{\mathbf{p}}$ is the nucleon energy. Eq. (2) is Fermi’s golden rule with final–state nucleon blocking. The energy delta function expresses energy conservation and momentum conservation, comes from the matrix elements of the nucleon density operators $\langle p' | \int d^3x e^{i\mathbf{q}\cdot\mathbf{x}} n(\mathbf{x}) | p \rangle$, and has already been integrated out. From the δ function in (5) we see that a typical energy transfer ω from the medium to the neutrino is of the order of q times the thermal velocity, $(T/m)^{1/2}$. Thus, in the limit of heavy nucleons, when we integrate the differential rate (2) over a range of ω s the other factors in the integrand can be evaluated at $\omega = 0$. We can express this limit as,

$$(2\pi)^{-1}S(q, \omega) \rightarrow (2\pi)^{-1}\delta(\omega) \int d\omega' S(q, \omega') \equiv \delta(\omega)S(q), \quad (6)$$

where $S(q)$ is the *static* structure factor. In §VI, we show that at the high densities and temperatures achieved in the supernova context the $\omega = 0$ (elastic) limit is not particularly accurate (see also [30]).

When we turn on interactions among the nucleons, (5) is replaced by,

$$S(q, \omega) = 2\pi Z^{-1} \sum_{j,k} e^{-\beta E_j} \int d^3x e^{i\mathbf{q}\cdot\mathbf{x}} \langle j | n(\mathbf{x}) | k \rangle \langle k | n(0) | j \rangle \delta(\omega + E_j - E_k), \quad (7)$$

where j and k are energy eigenstates, now of the whole medium, Z is the partition function, T is the temperature, and $\beta = \frac{1}{T}$. If the medium is comprised of heavy enough nucleons, we need only the static structure function defined in (6), then given by

$$S(q) = Z^{-1} \sum_j e^{-\beta E_j} \int d^3x e^{i\mathbf{q}\cdot\mathbf{x}} \langle j | n(\mathbf{x}) n(0) | j \rangle. \quad (8)$$

In other words, $S(q)$ is merely the Fourier transform of the thermally–averaged density–density correlation function. This is the classic result that scattering off of a medium is in reality scattering off of the *fluctuations* in that medium. Also of interest is the long–wavelength limit, $q \rightarrow 0$, justified when the neutrino wavelength is much bigger than the interparticle separation.¹ Statistical mechanics provides two useful and equivalent expressions for the long–wavelength limit, $S(0)$, the first [33] in terms of the isothermal compressibility of the medium $K_T (= -\frac{\partial \log V}{\partial P}|_T)$,

$$S(0) = \bar{n}^2 \beta^{-1} K_T = \bar{n} \frac{K_T}{K_0}, \quad (9)$$

where K_0 is the ideal gas compressibility and \bar{n} is the average nucleon density, and the second (*ibid.*, their eq. 114.14) in terms of the derivative of the density with respect to the chemical potential of the nucleons, μ ,

¹We emphasize that the limits discussed in this section are presented both for pedagogical reasons and because they provide a boundary condition for the later work in this paper, in which we require neither limit. Under the actual conditions that prevail in the supernova core the conditions for the limits to be applicable are marginally satisfied, at best.

$$S(0) = \beta^{-1} \frac{\partial \bar{n}}{\partial \mu}. \quad (10)$$

In the ideal gas limit of no correlation between particles, eqs. (9) and (10) show that $S(q)$ is simply equal to the number density, \bar{n} , as expected from eq. (8) and eq. (5), without blocking. Eq. (9) reveals that if K_T is small because the matter is stiff, in the long-wavelength limit the neutrino-matter cross sections are *suppressed*. When we replace eq. (1) by the complete standard model form, including the axial-vector current and nucleon isospin, we shall require separate correlation functions for the neutron and the proton, as well as for spin correlations. These depend upon susceptibilities that are different from the compressibility, but we shall find suppression in these terms as well.

Eq. (10), equivalent to eq. (9) by a thermodynamic identity, is a powerful result of great generality. In standard approximation schemes for the many-body problem, the distribution function for a nucleon species is given by the Fermi-Dirac distribution in which the chemical potential μ is replaced by $\mu - v(\bar{n})$, where $v(\bar{n})$ is the average energy of interaction of the nucleon with the other nucleons and is a function of the density. Thus, the density is given implicitly by

$$\bar{n} = 2 \int \frac{d^3 p}{(2\pi)^3} [1 + e^{\beta[(p^2/(2m) - \mu + v(\bar{n}))]}]^{-1}. \quad (11)$$

The expression (11) holds in the Hartree approximation; it holds in approaches that introduce mean meson fields instead of nuclear potentials; it holds in the Landau Fermi liquid theory (FLT), subject to the proviso that we use only results in which the derivative of the potential v (with respect to the \bar{n}) enters; and it holds in approaches using the Skyrme potential.

Differentiating (11), we can solve for $\frac{\partial \bar{n}}{\partial \mu}$ and $S(0)$,

$$S(0) = \beta^{-1} \frac{\partial \bar{n}}{\partial \mu} = h(\mu) [1 + h(\mu) \frac{\partial v}{\partial \bar{n}}]^{-1}, \quad (12)$$

where

$$h(\mu) = 2 \int \frac{d^3 p}{(2\pi)^3} \frac{e^{\beta[p^2/(2m) - \mu + v]}}{[1 + e^{\beta[p^2/(2m) - \mu + v]}]^2} = 2 \int \frac{d^3 p}{(2\pi)^3} f_1(p) (1 - f_1(p)) \quad (13)$$

and $f_1(p)$ is the Fermi-Dirac function, but with the chemical potential displaced by v . If we regard particle densities as inputs to our calculations, then the displacement of the chemical potential by the nuclear potential is irrelevant, since the same difference, $\mu - v$, enters the calculation of the density in terms of the chemical potential. Thus, the numerator of (12) contains no more than the familiar Pauli blocking effects (for the case $q = 0$); the denominator contains all of the effect of the interactions.

As an example, consider a two-nucleon potential $V(r)$. In the Hartree approximation, the average potential seen by a single nucleon is given by $v = \bar{n}U$, where $U = \int d^3 x V(x)$, and (12) becomes

$$S(0) = h(\mu) [1 + h(\mu)U]^{-1}, \quad (14)$$

the potential providing an enhancement, if negative, and a suppression, if positive. The latter is the case for high-density nuclear matter.

Extensions of the above considerations to include isotopic spin and the axial-vector weak hadronic current were given in reference [34]. Closely related considerations were given in reference [21] for the case of degenerate neutron matter. Both references [34] and [21] concluded that nuclear interactions cause a big decrease in the Gamow-Teller part of the neutrino opacity in the regions considered in the respective works. However, in addition to being fragmentary in the domains that were covered, these works did not address two important issues: 1) the errors in doing the integral over ω by assuming that the neutrino parts of the matrix element and phase space factors are independent of ω over the region of dominant contribution and, 2) the applicability of the $q = 0$ limit. These limits are the least justified for the case of trapped electron neutrinos in the early dense core, where the momentum transfers in neutrino scattering are comparable to the inverse particle spacing.

In the present work we address these deficiencies by using methods that incorporate all of the physics of the above discussion and previously cited papers, but which calculate the dynamic structure factor as a function of (q, ω) and do the integrals over the neutrino variables, without further approximation. We also aim to better systematize the problem by keeping the connections to textbook many-body formalism ² as clear as possible.

III. GENERAL FORMULATION

To address in complete form the reactions that a neutrino undergoes in a medium we need to calculate the appropriate thermal averages of the weak-current operators for the particles that comprise the medium. We define j_μ as the weak neutral current of the particles in the medium, other than the neutrinos, and we assume conditions under which all species, except the neutrinos, are in statistical equilibrium. The properties of the medium are embodied in the function $W_{\mu\nu}$

$$W_{\mu\nu}(q, \omega) = \mathcal{F}[j_\mu, j_\nu]_{q, \omega}, \quad (15)$$

where we define the correlation functional $\mathcal{F}_{q, \omega}$ of two Heisenberg operators O_1 and O_2 as

$$\mathcal{F}[O_1, O_2]_{q, \omega} = Z^{-1} \int d^4x e^{-i\mathbf{q}\cdot\mathbf{x}} e^{i\omega t} \text{Tr}[e^{-\beta(H - \Sigma\mu_i N_i)} O_1(\mathbf{x}, t) O_2(\theta, \theta)], \quad (16)$$

where Z is the partition function. We can write the differential rate for neutrino scattering in terms of $W_{\mu\nu}(q, \omega)$,

$$\frac{d^2\Gamma}{d\omega d\cos\theta} = (4\pi^2)^{-1} G_W^2 (E_1 - \omega)^2 [1 - f_\nu(E_1 - \omega)] \Lambda^{\mu\nu}(q, \omega) W_{\mu\nu}(q, \omega). \quad (17)$$

Note that the leptonic spinor-trace and phase-space factors are as in the golden rule formula (2). The distribution functions for initial and final nucleon states, and the golden-rule delta function, have all been subsumed in $W_{\mu\nu}(q, \omega)$. When the medium is interacting,

²In what follows, we will use a number of formulae from Fetter and Walecka [35], hereafter referred to as FW.

(17) can be taken as the definition of the correct answer, as it is in the form that *ab initio* thermal field theory gives for neutrino transition rates. Alternatively, when a complete set of intermediate energy and momentum eigenstates are inserted between the two operators in (16), the d^4x integrals give the delta functions, the two matrix elements give the square of the T matrix, and the thermal factor weights them appropriately, as in (7).

We take the medium to be composed of protons, neutrons, electrons and neutrinos and we deal only with the neutrino scattering from the nucleons in the medium.³

For the nuclear contribution, we assume that the nucleons remain non-relativistic to write the space components of the function $W_{\mu\nu}$ in the form,

$$W_{i,0} = W_{0,i} = 0 \quad W_{i,j}(q, \omega) = W_A(q, \omega)\delta_{i,j} + W_B(q, \omega)q_i q_j. \quad (18)$$

We define $W_V = W_{0,0}$. The lepton trace can be expressed in terms of these functions as follows,

$$W_{\mu\nu}\Lambda^{\mu\nu} = (1 + \cos\theta)W_V + (3 - \cos\theta)W_A + \omega^2(1 + \cos\theta)W_B, \quad (19)$$

where, as before, θ is the scattering angle, W_V represents the Fermi (vector) term, and W_A is the Gamow–Teller (axial–vector) term.

The W_B term in eq. (19) vanishes in the absence of interactions among the nucleons. In our later parameterization of the forces, it can become different from zero only when a tensor force is added to the conventional four central forces. We have directly evaluated the contribution to the opacity from the tensor force coming from single neutral–pion exchange and find, for degenerate matter around nuclear density, $W_B \approx 2 \times 10^{-5}W_A(\text{MeV})^{-2}$. The tensor terms give an additional opacity that is a small fraction of that due to the axial–vector terms (W_A), and we drop them in what follows.

The non–relativistic limits of the standard model neutral current to be used in (15) can be expressed in terms of the neutron and proton density operators, n_n and n_p , and the \hat{z} component of the spin–density operators, $n_{n,p}^{(3)} = \psi_{n,p}^\dagger \sigma_3 \psi_{n,p}$,

$$\begin{aligned} j_0(x) &= C_V^{(p)} n_p(x) + C_V^{(n)} n_n(x) \\ j_3(x) &= g_A(n_p^{(3)}(x) - n_n^{(3)}(x)), \end{aligned} \quad (20)$$

where $C_V^{(p)} = 1/2 - 2 \sin^2 \theta_W$, $C_V^{(n)} = 1/2$, $g_A = -1.26/2$, and $\sin^2 \theta_W = 0.23$. By rotational invariance, we need only the correlation functions of the \hat{z} component of the spin, but, since the medium is not invariant under isospin rotations, we use separate neutron and proton currents.

For the vector (Fermi) part, we now obtain,

$$W_V(q, \omega) = (C_V^{(p)})^2 S_{pp}(q, \omega) + 2C_V^{(p)} C_V^{(n)} S_{pn}(q, \omega) + (C_V^{(n)})^2 S_{nn}(q, \omega), \quad (21)$$

³Of course, neutrino–electron scattering through the neutral–current couplings must be taken into account in the determination of the total opacity, and for the case of electron neutrinos the charged–current interactions with nucleons and with electrons must be used as well.

where the structure functions are defined as $S_{pp} = \mathcal{F}[n_p, n_p]$, $S_{pn} = \mathcal{F}[n_p, n_n]$, and $S_{nn} = \mathcal{F}[n_n, n_n]$.

For the axial–vector (Gamow–Teller) part, we have

$$W_A(q, \omega) = g_A^2(S_{pp}^A(q, \omega) + S_{nn}^A(q, \omega) - 2S_{pn}^A(q, \omega)) = g_A^2 S_A(q, \omega), \quad (22)$$

where $S_{pp}^A = \mathcal{F}[n_p^{(3)}, n_p^{(3)}]$, $S_{pn}^A = \mathcal{F}[n_p^{(3)}, n_n^{(3)}]$, and $S_{nn}^A = \mathcal{F}[n_n^{(3)}, n_n^{(3)}]$. The purpose of the remainder of this paper is to calculate the six structure functions.

A. An Aside on the Long–Wavelength Limit

In the long–wavelength limit, we can calculate the six structure functions quite simply and intuitively. We introduce the average densities, \bar{n}_i , for the four species, $\bar{n}_i = (Vol)^{-1} \int d^3x n_i(x)$, where the index i runs over the values p^\uparrow , p^\downarrow , n^\uparrow , n^\downarrow , and we form the combinations,

$$\begin{aligned} \bar{n}_{p,n} &= \bar{n}_{p,n}^\uparrow + \bar{n}_{p,n}^\downarrow \\ \bar{n}_{p,n}^A &= \bar{n}_{p,n}^\uparrow - \bar{n}_{p,n}^\downarrow. \end{aligned} \quad (23)$$

We also introduce separate chemical potentials for the up and down spin states for the two species and introduce the notations,

$$\begin{aligned} \mu_{p,n} &= \frac{1}{2}(\mu_{p,n}^\uparrow + \mu_{p,n}^\downarrow) \\ \mu_{p,n}^A &= \frac{1}{2}(\mu_{p,n}^\uparrow - \mu_{p,n}^\downarrow). \end{aligned} \quad (24)$$

Then, as shown in (10) and reference [34], we can express the $q \rightarrow 0$ limits of the static structure functions as follows:

$$\begin{aligned} S_{pp}(0) &= \beta^{-1} \frac{\partial \bar{n}_p}{\partial \mu_p} \quad ; \quad S_{nn}(0) = \beta^{-1} \frac{\partial \bar{n}_n}{\partial \mu_n} \\ S_{pn}(0) &= S_{np}(0) = \beta^{-1} \frac{\partial \bar{n}_p}{\partial \mu_n} \\ S_{pp}^A(0) &= \beta^{-1} \frac{\partial \bar{n}_p^A}{\partial \mu_p^A} \quad ; \quad S_{nn}^A(0) = \beta^{-1} \frac{\partial \bar{n}_n^A}{\partial \mu_n^A} \\ S_{pn}^A(0) &= S_{np}^A(0) = \beta^{-1} \frac{\partial \bar{n}_p^A}{\partial \mu_n^A}. \end{aligned} \quad (25)$$

As in the one–channel case treated in §II, we take the distribution function for a nucleon species, i , to be given by the Fermi–Dirac distribution in which the chemical potential, μ_i , has been replaced by $\mu_i - v_i$, where v_i is the average energy of interaction of the nucleon with all other particles. Thus, the density is given by

$$\bar{n}_i = 2 \int \frac{d^3p}{(2\pi)^3} [1 + e^{\beta(p^2/(2m) - \mu_i + v_i)}]^{-1}. \quad (26)$$

In general, the potential, v_i for species i is a function of the densities for all four of the species, \bar{n}_j . If we know the functional dependence of the v 's on the \bar{n}_j s, we can solve for the long–wavelength limit of the Fermi static structure functions, S , by differentiating the

four equations (26), with respect to the four chemical potentials that we have introduced. We give the solution for the two combinations of structure functions that enter our rate calculations. In (21), with $\sin^2 \theta_W = 1/4$, we have only the neutron contribution,

$$S_{nn} = \beta^{-1} \frac{\partial \bar{n}_n}{\partial \mu_n} = h(\mu_n)/d_V, \quad (27)$$

where

$$d_V = 1 + \frac{\partial v_n}{\partial \bar{n}_n} h(\bar{n}_n) - \left[\frac{\partial v_n}{\partial \bar{n}_p} \right]^2 h(\mu_n) h(\mu_p) \left[1 + \frac{\partial v_p}{\partial \bar{n}_p} h(\mu_p) \right]^{-1}. \quad (28)$$

In (22), integrated over ω , we obtain a simple form, if we choose potentials v_i such that $\partial v_i / \partial \bar{n}_j = \partial v_j / \partial \bar{n}_i$ and such that $v_{p\uparrow} - v_{p\downarrow} + v_{n\uparrow} - v_{n\downarrow} = 0$, two conditions that are fulfilled by the potentials we use. We then obtain,

$$S_A(q) = S_{pp}^A(q) + S_{nn}^A(q) - 2S_{pn}^A(q) = \frac{h(\mu_p) + h(\mu_n)}{1 + v_a(h(\mu_p) + h(\mu_n))}, \quad (29)$$

where $v_a = \frac{1}{8} \left[\frac{\partial}{\partial \bar{n}_p^A} - \frac{\partial}{\partial \bar{n}_n^A} \right] [v_{p\uparrow} - v_{p\downarrow} - v_{n\uparrow} + v_{n\downarrow}]$.

We present these static, long-wavelength results (eqs. 27 and 29), which depend on effective single-particle potentials, because they show a strong similarity in form to the more complete equations that will be developed in the next section and because, in most regions, they give numerical results that are not greatly different. However, it should be pointed out that any program that begins with potentials that fit nuclear data and calculates the ground-state properties of nuclear matter (*cf.*, [36,37]) is capable, if subjected to the right sets of constraints, of directly determining the low-temperature values of the static structure functions enumerated in (25), without recourse to the assumptions that led to eqs. (27) and (29). Implementation requires use of the multichannel analogues of the connection between the one-species structure function and the bulk modulus (9). The required numerical experiment involves constraining the system to have different expectation values of proton spin and neutron spin densities (in the \hat{z} direction), calculating the constrained ground-state energy as a function of these densities (as well as the particle densities), and taking combinations of second derivatives of this energy with respect to the densities, evaluated finally for the values of the densities in the true ground state. We strongly recommend that groups that do nuclear matter calculations carry out these steps.

IV. COMPLETE CORRELATION FUNCTIONS

In the field-theoretic formalism for the quantum mechanical many-body problem there are well-formulated perturbative techniques for directly calculating correlation functions, without restricting to the equal time ($\omega = 0$) and $q \rightarrow 0$ limits. In Appendix B, we show that the limiting results sketched out in the previous section by calculating the derivatives, $\frac{\partial \bar{n}_i}{\partial \mu_i}$, are exactly what we obtain, in the same limits, from the sum of the “ring” approximation graphs in this many-body formalism. Therefore, we must sum at least the ring graphs to recapture the long-wavelength limit of the static structure function. In so doing, we obtain

the full dynamic structure function $S(q, \omega)$ at the same level at which we find the limiting forms in §III.A.

To follow a graph summing approach we must replace the “correlation functional” of two (bosonic) operators defined in (16), \mathcal{F} , by a retarded commutator form, $\tilde{\mathcal{F}}$,

$$\tilde{\mathcal{F}}[O_1, O_2]_{q, \omega} = -\frac{i}{Z} \int d^4x e^{-i\mathbf{q}\cdot\mathbf{x}} e^{i\omega t} \text{Tr}[e^{-\beta(H - \Sigma\mu_i N_i)} [O_1(\mathbf{x}, t), O_2(\theta, \theta)]] \theta(t), \quad (30)$$

where here $\theta(t)$ is the Theta function.

The “correlation functional,” eq. (16), is recaptured through (FW eqs. 32.14 and 32.16),

$$\mathcal{F}_{q, \omega} = 2\text{Im}[\tilde{\mathcal{F}}_{q, \omega}](1 - e^{-\beta\omega})^{-1}. \quad (31)$$

Reverting to the single-channel problem for illustrative purposes, we define the polarization function as

$$\Pi(q, \omega) = \tilde{\mathcal{F}}[n, n]_{q, \omega}, \quad (32)$$

so that

$$S(q, \omega) = 2\text{Im}[\Pi(q, \omega)](1 - e^{-\beta\omega})^{-1}. \quad (33)$$

Note that we can use the fact that $\text{Im}\Pi(q, \omega)$ is odd in the variable, ω , to derive from (33) the relation that embodies detailed balance, $S(-\omega) = e^{-\beta\omega}S(\omega)$. The ring approximation (sometimes referred to as the Random Phase Approximation, RPA) then gives

$$\Pi(q, \omega) = \frac{\Pi^{(0)}(q, \omega)}{1 - v(q)\Pi^{(0)}(q, \omega)}, \quad (34)$$

where $v(q) = \int d^3x V(x)$ and $\Pi^{(0)}(q, \omega)$ is the free polarization. Eq. (34) is of the same general form as eq. (12) for the equal-time and small- q limits. If we take only the numerator in (34), we recover the effects of Pauli blocking alone.

To complete the calculation, we need the real and imaginary parts of $\Pi^{(0)}(q, \omega)$, which we derive in Appendix A:

$$\text{Re } \Pi^{(0)}(q, \omega) = \frac{m^2}{2\pi^2 q \beta} \int_0^\infty \frac{ds}{s} \log \left[\frac{1 + e^{-(s+Q)^2 + \beta\mu}}{1 + e^{-(s-Q)^2 + \beta\mu}} \right] + (\omega \rightarrow -\omega) \quad (35)$$

and

$$\text{Im}\Pi^{(0)}(q, \omega) = \frac{m^2}{2\pi\beta q} \log \left[\frac{1 + e^{-Q^2 + \beta\mu}}{1 + e^{-Q^2 + \beta\mu - \beta\omega}} \right], \quad (36)$$

where

$$Q = \left(\frac{m\beta}{2}\right)^{1/2} \left(-\frac{\omega}{q} + \frac{q}{2m}\right) \quad (37)$$

and for m we should substitute the effective mass, m^* [30].

To obtain the various $S(q, \omega)$ functions that are used in (34) for determining the rates, the above formulae are generalized to the multiple-channel case by considering the correlations of every pair of densities from the set n_p, n_n, n_p^3, n_n^3 . The cross correlations between the densities and the spin densities, n_i^3 , vanish, as do all dynamical connections between the two at the ring level, so that we are left with two 2×2 problems in solving for the correlations. In each sector, we define a matrix polarization function $\Pi(q, \omega)_{i,j} = \tilde{\mathcal{F}}[n_i, n_j]_{q,\omega}$ and a ring approximation, which is the simple matrix extension of (34). For the free polarization matrix, $\Pi^{(0)}$, we take a diagonal matrix in which the proton and neutron elements are given by (35) and (36), with the respective proton and neutron chemical potentials, μ_p and μ_n , in place of μ . The generalization of the potential, v , will connect the proton and neutron elements. The elements of the structure function matrices, S and S^A , used in the rate formulae follow immediately from the matrix form of (34). It remains to address the potentials.

A. Nucleon Potential Model

A general velocity-independent local two-body interaction between nucleons (a) and (b) is given by,

$$V^{a,b} = V_1(r) + \vec{\tau}^a \cdot \vec{\tau}^b V_2(r) + \vec{\sigma}^a \cdot \vec{\sigma}^b V_3(r) + \vec{\tau}^a \cdot \vec{\tau}^b \vec{\sigma}^a \cdot \vec{\sigma}^b V_4(r). \quad (38)$$

This leads directly to the following construction: ⁴

a) to determine the Fermi $S(q, \omega)$ elements, we use

$$\begin{aligned} v_{pp}(q) &= v_{nn}(q) = v_1(q) + v_2(q) \\ v_{pn}(q) &= v_{np}(q) = v_1(q) - v_2(q) \end{aligned} \quad (39)$$

and b) to determine the Gamow-Teller $S^A(q, \omega)$ elements, we use

$$\begin{aligned} v_{pp}^A(q) &= v_{nn}^A(q) = v_3(q) + v_4(q) \\ v_{pn}^A(q) &= v_{np}^A(q) = v_3(q) - v_4(q). \end{aligned} \quad (40)$$

Of course, in the nuclear interaction problem within nuclei, as well as at the higher densities in neutron star matter, there are a few complications: 1) there isn't a potential, 2) taking one anyway, it is too strong to allow the use of perturbation theory ⁵, 3) the better numerical methods (*e.g.*, correlated basis functions) for determining the ground-state energy

⁴In interpreting these matrix elements it should be borne in mind that they are not analogous to matrix elements of an operator between single-particle states. They operate in a space of two neutral densities (the arguments of $\tilde{\mathcal{F}}$) and describe the scattering of two particles, with no charge exchange.

⁵For example, our plane-wave Hartree approximation, used with the potential that is attributed to ω -meson exchange, would give much too much positive energy and too great a rate reduction for the Fermi terms, since it doesn't keep the particles apart at short distances.

of nuclear matter from a phenomenological potential may be poorly adapted to calculation of the dynamic structure functions.

Since it is the excitations of the medium, rather than the cold equation of state, that really enter this problem, the Landau Fermi liquid theory provides a framework for proceeding. This theory defines an energy functional associated with variations of the various densities. We define combinations of density variations,

$$\begin{aligned}
\delta_{0,0} &= \delta n_p + \delta n_n \\
\delta_{3,0} &= \delta n_p - \delta n_n \\
\delta_{0,3} &= \delta n_p^\uparrow + \delta n_n^\uparrow - \delta n_p^\downarrow - \delta n_n^\downarrow \\
\delta_{3,3} &= \delta n_p^\uparrow - \delta n_n^\uparrow - \delta n_p^\downarrow + \delta n_n^\downarrow,
\end{aligned} \tag{41}$$

where the vertical arrows signify spin-up and spin-down densities. The absence of an arrow implies the sum of these densities.

The energy response to these variations that defines the FLT is given by

$$\begin{aligned}
\delta E &= \sum_{q,i} \epsilon_i^{(0)}(q) \delta n_i(q) + \frac{\lambda}{2} \sum_{q,q'} [\delta_{0,0}(\mathbf{q}) \delta_{0,0}(\mathbf{q}') F + \\
&\delta_{3,0}(\mathbf{q}) \delta_{3,0}(\mathbf{q}') F' + \delta_{0,3}(\mathbf{q}) \delta_{0,3}(\mathbf{q}') G + \delta_{3,3}(\mathbf{q}) \delta_{3,3}(\mathbf{q}') G'],
\end{aligned} \tag{42}$$

where $\lambda = \pi^2(2m^*p_F)^{-1}$ and p_F is the nucleon Fermi momentum. The FLT parameters are usually a function of the angle between q and q' . We shall consider the wavelength in our application to be long enough so that only the S-wave parameters, F_0, F'_0, G_0, G'_0 , enter. Then, we note that the interaction term, quadratic in the δ s, is exactly what one would get from the form (38), with zero-range two-body potentials, where we define $v_i = \int d^3r V_i(r)$, and obtain

$$v_1 = \lambda F_0; \quad v_2 = \lambda F'_0; \quad v_3 = \lambda G_0; \quad v_4 = \lambda G'_0. \tag{43}$$

Note that all the v_i s are real.

The parameter λ in (42) implies that our potential has a density dependence. However, we view this as simply part of the mechanics of fixing our parameters $\int d^3r V_i$ in terms of the hodgepodge of nuclear phenomenology, at nuclear densities, and meson-exchange considerations that went into the fixing of the FLT parameters. We keep the parameter p_F fixed at its value for nuclear density, and use our derived parameters at all densities. This is clearly a sounder procedure at or near nuclear densities, where unextrapolated phenomenology was the main input, but we shall calculate the results over a wide region of densities nonetheless. We note that the use of Skyrme interactions, expressing an effective energy functional as a form quadratic and cubic in the densities, would be subject to the same caveats.

For supernova and protoneutron star applications, we must include Coulomb forces in our interaction Hamiltonian. We can do so by adding to the (zero-range) proton-proton force in (39), a Thomas-Fermi screened Coulomb force between protons,

$$v_{pp} = \int d^3r V^{p,p} = v_1 + v_2 \rightarrow v_1 + v_2 + 4\pi e^2 (q^2 + q_{TF}^2)^{-1}, \tag{44}$$

where $q_{TF}^2 = 4e^2\pi^{1/3}(3\bar{n}_p)^{2/3}$. In the denser regions of the star, the screening momentum is larger than the q for typical neutrino scattering. In this case, the Coulomb term in (44) for the proton-proton interaction is independent of q and e^2 .⁶

V. FINAL PROCEDURE FOR CALCULATING ν -NUCLEON STRUCTURE FUNCTIONS

From eqs. (17), (19), (21), and (22) and taking only the neutron part of the vector-current coupling, the differential scattering rate is given by,

$$\begin{aligned} \frac{d^2\Gamma}{d\omega d\cos\theta} = & (4\pi^2)^{-1}G_W^2E_2^2[1 - f_\nu(E_2)]\left[(1 + \cos\theta)(C_V^n)^2S_{nn}(q, \omega) \right. \\ & \left. + (3 - \cos\theta)g_A^2[S_{pp}^A(q, \omega) + S_{nn}^A(q, \omega) - 2S_{pn}^A(q, \omega)], \right] \end{aligned} \quad (45)$$

where $E_2 = E_1 - \omega$.

The structure functions, S and S^A , are elements of separate 2×2 symmetric matrices. For the vector dynamic structure function, S , we have

$$S(q, \omega) = \begin{pmatrix} S_{pp}(q, \omega) & S_{pn}(q, \omega) \\ S_{pn}(q, \omega) & S_{nn}(q, \omega) \end{pmatrix}.$$

The structure function matrix is given by,

$$S(q, \omega) = 2\text{Im}\left[\Pi^{(0)}(q, \omega)[1 - v(q)\Pi^{(0)}(q, \omega)]^{-1}\right](1 - e^{-\beta\omega})^{-1} \quad (46)$$

where

$$\Pi^{(0)}(q, \omega) = \begin{pmatrix} \Pi_p^{(0)}(q, \omega) & 0 \\ 0 & \Pi_n^{(0)}(q, \omega) \end{pmatrix}$$

and $\Pi_p^{(0)}$ and $\Pi_n^{(0)}$ are given by the polarization function, defined in (35) and (36) and evaluated with the proton and neutron chemical potentials, respectively. The potential matrix is,

⁶The physics of this additional term can best be elucidated by considering for a moment what the effects would be if the Fermi term in our weak current coupled only to the protons in the medium (rather than almost entirely to the neutrons, as in the standard model.) In this case the scattering of neutrinos would be dominated by the scattering from proton-density fluctuations on the order of the neutrino wavelength. For long neutrino wavelengths, such fluctuations are strongly suppressed by the Coulomb force. When $q \ll q_{TF}$ the price paid in energy for the fluctuation is measured by the increase in the kinetic energies of the neutralizing electrons, and we note that in this limit the Coulomb term in (44) is just the second derivative of the electron Fermi energy with respect to electron (or proton) density. In the case at hand, where $\sin\theta_W \approx 1/2$ so that the weak coupling is entirely with the neutrons, the Coulomb force between protons turns out nonetheless to be quite important, because of the strong coupling of neutrons to protons in the symmetry-energy term.

$$v = \begin{pmatrix} v_1 + v_2 + 4\pi e^2(q^2 + q_{TF}^2)^{-1} & v_1 - v_2 \\ v_1 - v_2 & v_1 + v_2 \end{pmatrix},$$

where the v 's were defined in terms of Fermi liquid parameters in (43).

In a real calculation, in all the kinematic expressions m is to be replaced by m^* . Unfortunately, the relation of Landau parameters to experimental results depends upon the effective mass in model-dependent ways. Taking $m^* = 0.75m_n$ as our fiducial value for the effective mass, we use parameters from references [38,39]: $F_0 = -0.28$; $F'_0 = 0.95$; $G_0 = 0$; $G'_0 = 1.7$ and $\lambda = 2.63 \times 10^{-5} \text{MeV}^{-2}$, obtaining,

$$\begin{aligned} v_1 &= -7.4 \times 10^{-6} \text{MeV}^{-2} \\ v_2 &= 2.5 \times 10^{-5} \text{MeV}^{-2} \\ v_3 &= 0 \\ v_4 &= 4.5 \times 10^{-5} \text{MeV}^{-2}. \end{aligned} \tag{47}$$

For other values of the effective mass, we keep these potentials at the same value, which is to say we assume that the Landau parameters are proportional to m^*/m . For the dominant spin-independent term, v_2 , this accords with the conventional wisdom that the symmetry energy per nucleon can be written in the form $\alpha((A-Z)/N)^2$.

The form for the Gamow-Teller matrix, $S^A(q, \omega)$, is the same as that for S , except that the potential matrix is replaced by v^A

$$v^A = \begin{pmatrix} v_3 + v_4 & v_3 - v_4 \\ v_3 - v_4 & v_3 + v_4 \end{pmatrix}.$$

Taking the matrix inverses leads to the following forms for the combinations of structure functions that appear in (45)

$$S_{nn}(q, \omega) = 2\text{Im}[\Pi_n^{(0)} D_V^{-1}](1 - e^{-\beta\omega})^{-1}, \tag{48}$$

where

$$D_V = 1 - (v_1 + v_2)\Pi_n^{(0)} - (v_1 - v_2)^2\Pi_n^{(0)}\Pi_p^{(0)}[1 - 4\pi e^2(q^2 + q_{TF}^2)^{-1}\Pi_p^{(0)} - (v_1 + v_2)\Pi_p^{(0)}]^{-1}, \tag{49}$$

which corresponds in the $(q, \omega) \rightarrow (0, 0)$ limits to eq. (27).

If, as in (47), we take $v_3 = 0$, we obtain the simple result for the axial-current terms,

$$S_A(q, \omega) = 2\text{Im}\left[\frac{\Pi_p^{(0)}(q, \omega) + \Pi_n^{(0)}(q, \omega)}{1 - v_4[\Pi_p^{(0)}(q, \omega) + \Pi_n^{(0)}(q, \omega)]}\right](1 - e^{-\beta\omega})^{-1}, \tag{50}$$

which corresponds in the $(q, \omega) \rightarrow (0, 0)$ limits to eq. (29).

VI. RESULTS

The formulae that we have developed to calculate dynamic structure functions and scattering rates (*i.e.*, cross sections) for neutrino-matter scattering in nuclear matter, in particular eqs. (45), (48), and (50), can now be used to obtain quantitative results. One is free to

insert whatever parameters for whatever thermodynamic states and nuclear models, but we here choose to focus on a generic subset of possibilities to demonstrate the character of the new results. Since there are six neutrino species in thermal equilibrium in the supernova core and the electron types have very different chemical potentials than the ν_μ s and ν_τ s, we drop the blocking term, $(1 - f_\nu(E_2))$, in calculating the total suppression factors. This term is trivial to include in the general case, and for the ν_μ s and ν_τ s its omission introduces only a small error. However, we want to avoid expanding the number of comparisons unduly and the reader is free to employ the derived equations to calculate everything for any combination of parameters. Since for the differential cross sections one does not integrate over the energy transfer, ω , and we present not absolute cross sections, but cross sections normalized to the non-interacting case, the differential cross section results are fully general. Final-state nucleon blocking is always included.

For the Fermi term, since $C_V^{(p)} = 1/2 - 2\sin^2\theta_W \sim 0$, we drop the proton structure function in (45). Furthermore, we use the potential parameters given in eq. (47), and in eq. (49) we drop the third term. This term would have been significant had it not been for the Coulomb term in the denominator, an illustration of the importance of the explicit inclusion of Coulomb forces, even for the neutron density correlations. Since the v_i s are all real, we obtain for the structure factors used in (45),

$$S_F(q, \omega) = 2\text{Im}\Pi_n^{(0)}(1 - e^{-\beta\omega})^{-1}\mathcal{C}_V^{-1}, \quad (51)$$

where

$$\mathcal{C}_V = (1 - v_F\text{Re}\Pi_n^{(0)})^2 + v_F^2(\text{Im}\Pi_n^{(0)})^2, \quad (52)$$

and

$$S_A(q, \omega) = 2[\text{Im}\Pi_p^{(0)}(q, \omega) + \text{Im}\Pi_n^{(0)}(q, \omega)](1 - e^{-\beta\omega})^{-1}\mathcal{C}_A^{-1}, \quad (53)$$

where

$$\mathcal{C}_A = [1 - v_{GT}(\text{Re}\Pi_p^{(0)}(q, \omega) + \text{Re}\Pi_n^{(0)}(q, \omega))]^2 + v_{GT}^2[\text{Im}\Pi_p^{(0)}(q, \omega) + \text{Im}\Pi_n^{(0)}(q, \omega)]^2. \quad (54)$$

The F in $S_F(q, \omega)$ and the A in $S_A(q, \omega)$ stand for Fermi and Gamow–Teller (axial) and v_F and v_{GT} equal $(v_1 + v_2)$ and v_4 , respectively. $\mathcal{C}_{V,A}$ is the correction factor due to many-body effects for a given momentum transfer (or scattering angle) and energy transfer.

A. Collective Excitations of the Medium

For most regions of phase space, \mathcal{C}_A and \mathcal{C}_V are greater than one and represent suppression in the scattering rates. Their effects on the integrals over ω and θ are always suppressive. However, the terms containing the real parts have roots; these roots represent collective excitations. For the Fermi term, zero sound in the medium can be generated if the scattering has a (ω, q) pair that satisfies the mode's dispersion relation, *i.e.*, if it hits the resonance. Similarly, for the Gamow–Teller term, spin waves in the protons and the neutrons (related by a set phase) can be generated. These modes are the traveling-mode equivalents of the Gamow–Teller resonance in nuclei (a standing wave). The zero sound of the Fermi part is

analogous to the Giant–Dipole resonance in nuclei. The resonances increase the structure function when the scattering transfer ratio, ω/q , equals the ratio of the collective excitation’s angular frequency and wavenumber. For a given scattering angle, one can plot the differential cross section in ω and $\cos\theta$ as a function of ω/q to see the resonances. In Figure (1), we display this for five different angles between 15° and 180° , an incident neutrino energy of 20 MeV, a temperature of 5 MeV, a density of 3×10^{14} gm cm $^{-3}$, and an electron fraction, Y_e , of 0.3. We see in Figure 1 that the resonances in both the forward and the backward directions line up at the same values of ω/q , as expected for a collective mode, and we can straightforwardly calculate the mode’s dispersion relation. This is akin to the Čerenkov effect. Note that the Gamow–Teller term dominates the Fermi term, so that in Figure 1 we are really seeing the spin waves related to the Gamow–Teller resonance. However, the dispersion relations for zero sound and these spin waves are generally similar. In fact, recalling the classic result [35] that in the weak–coupling limit, the speed of zero sound in a degenerate system is $\sim v_{fermi}$, where v_{fermi} is the Fermi velocity, and recalling that for nucleons in nuclei v_{fermi} is $\sim 0.3c$, the calculated resonance value of ω/q is not unexpected. In Figure 2, we plot the Gamow–Teller structure function versus ω/q for various values of ω , m^* , and two values of the density. At $m^* = m_n$, for each value of the density we obtain a sharp resonance, but at two different speeds, reflecting the crude $\rho^{1/3}$ –dependence expected for v_{fermi} . For a given density, the mode speed is seen in Figure 2 to be inversely proportional to the effective mass. The width of the resonance is determined by the magnitude of the imaginary part of the polarization function.

B. Differential Scattering Cross Sections and Suppression Factors

To calculate the singly–differential scattering cross sections ($d\sigma/d\omega$), we must integrate (45) over $\cos\theta$. Since for a given ω and incident neutrino energy, E_1 , this integration is also over a range of qs , in the process we are smoothing over resonances. As a consequence, there is no obvious direct signature of them in the final result. It is the doubly–differential structure functions and cross sections that retain the character of the collective modes and resonance. The integral over the singly–differential scattering cross section yields the total cross section, and this can be compared to that without correlations to gauge the magnitude of the suppression of the rate. To demonstrate the nature of the correlation effects, we have opted to present figures and tables for a subset of the possible ρ – T – Y_e – E_1 combinations. Recall that for this purpose we have employed the default potentials (47) and effective mass ($m^* = 0.75m_n$). Note, however, that the formalism we have derived is fully general, as long as the nucleons can be assumed to be non–relativistic and we are in the perturbative limit. Since we calculate at given neutron and proton densities, μ_n and μ_p are implicit in the formalism, as would be the shifts in them due to interactions [30].

We depict in Figure 3 the singly–differential scattering cross section, divided (normalized) by the total scattering cross section off of nucleons (σ_1), for a range of incident neutrino energies. We have used eqs. (45), (51), (52), (53), and (54) to generate these curves. Figure 3 is a study of the dependence on incident neutrino energy (1, 5, 10, 20, 30 MeV), at a fiducial (but arbitrary) density ($\rho = 3 \times 10^{14}$ gm cm $^{-3}$), temperature ($T = 5$ MeV), and electron fraction ($Y_e = 0.3$). Also shown as dashed lines are the corresponding curves without the many–body correlation effects ($\mathcal{C}_{\nu,\mathcal{A}}$) and for $m^* = m_n$, but with final–state nucleon blocking.

Table I depicts the corresponding many-body suppression factors, obtained by integrating under the curves, as well as both the average energy transfers ($\langle \omega \rangle$) and the *rms* of the energy transfers (ω_{rms}). Without neutrino blocking, the total suppressions we present in the tables are very close to the full results for ν_μ s and ν_τ s. For ν_e s, it is more important to include the $(1 - f_\nu(E_2))$ term, since there is a net electron lepton number in protoneutron stars for most of their interesting lives. Figure 3 is rich with information that we will try to summarize. Positive ω represents energy lost from the neutrino and negative ω represents energy gained by the medium. First, notice that the widths of the curves increase with the incident neutrino energy. Even for the curves without many-body effects, the widths as depicted in Figure 3 and in Table I are quite large. Such widths call into question the elastic approximation [26,28], but also imply that energy equilibration for the ν_μ s and ν_τ s by ν -nucleon scattering dominates over the annihilation process, $\nu + \bar{\nu} \rightarrow e^+ + e^-$, and ν -electron scattering, both with much lower cross sections [29]. Equilibration for the ν_e s is still via the charged-current absorption process, $\nu_e + n \rightarrow e^- + p$.

One major reason the widths are larger than are familiar is that in the past people thought that the neutrino could lose in ν -nucleon scattering an energy equal to only about $-E_1^2/m_n c^2$, *i.e.* that the fractional energy lost is of order $p_\nu/m_n c$ ($\sim 1\%$). However, this assumes that the nucleons are stationary. In fact, they are thermal and, the fractional energy they can transfer in a collision to the neutrino is of order $p_n/m_n c$. Since the nucleons have such a large mass, if they and the neutrino have the same energy, $p_n/m_n c$ is much larger than $p_\nu/m_n c$, at incident neutrino energies of 10–30 MeV by as much as an order of magnitude. The formalism we employ incorporates the kinematics of such a collision, a realistic Fermi-Dirac energy distribution for the nucleons, and final-state nucleon blocking. The upshot is the broad distributions, even without the $\mathcal{C}_{\nu,A}$, seen in Figure 3 and tabulated in Table I. Including many-body effects further flattens and broadens the distribution (see below), while lowering the central values of $d\sigma/d\omega$, as well as the total integral over ω .

As Table I demonstrates, even without many-body effects, nucleon blocking is a large effect, larger than the elastic $\frac{3}{2} \frac{T}{\mu_n}$ correction that comes from the low-temperature expansion in powers of T . That correction can be applied in the extreme degenerate limit, but the nucleons are only partially degenerate in protoneutron stars and supernovae, even at nuclear densities, and the extreme degenerate limit is never achieved. The error in using the $\frac{3}{2} \frac{T}{\mu_n}$ correction ansatz can be as much as a factor of two, depending upon the nuclear interaction model.

Note in Table I that the many-body cross section suppression factors are not strong functions of the incident neutrino energy, except at very low energies (*e.g.*, 1 – 5 MeV), but that the suppression factors themselves are quite large at this fiducial thermodynamic point (near nuclear density). The extra suppression, beyond that due to nucleon blocking, is due both to the decrease in the effective mass (factor of ~ 1.5) and to the many-body correlation terms, $\mathcal{C}_{\nu,A}$. The total factor is between 10 and 30. This means that the combination of final-state nucleon blocking (a factor of ~ 6 by itself) and many-body effects (another factor of 3 to 4) renders the supernova core much more transparent to neutrinos than previously thought. We remind the reader that we are here calculating only the neutral-current rates. While they dominate for the ν_μ s and ν_τ s, the charged-current dominates for the ν_e s. Nevertheless, we are in the midst of preliminary calculations that indicate that the suppression of these rates is also quite large (Burrows & Sawyer, in preparation; see also

Reddy *et al.*, in preparation).

The previous assumptions concerning the distribution in energy transfers for ν -nucleon scattering were more akin to the narrow (quasi-delta function) curve, seen in Figure 3 for 1-MeV incident neutrino energy. The contrast between that curve and the others is manifest.

Figure 4 is similar to Figure 3, but for a range of temperatures (5, 7, 10, 15, 20, 30 MeV). The calculations were done at $E_1 = 20$ MeV. Superposed are the corresponding reference curves for $\mathcal{C}_{\nu,A} = 1$ and $m^* = m_n$. Table II lists the suppression factors, $\langle \omega \rangle$, and ω_{rms} . As the temperature rises, the suppression diminishes. It is clear in Figure 4 that energy transfer from the medium to the neutrino becomes more likely as the temperature rises. This is to be expected and is all the more pronounced in the many-body case. As in Figure 3, the differential cross section is flattened when interaction effects are included, but Figure 4 shows that this flattening effect is more significant at higher temperatures. As Table II demonstrates, though the total suppression diminishes with temperature, many-body effects still increase it, the more so at lower temperatures. Given the large values of $\langle \omega \rangle$ and ω_{rms} , it is difficult to see how even a Fokker-Planck treatment of neutrino energy redistribution via these processes could be viable and the full redistribution formalism [40,41] may be required, at least for the ν_μ s and the ν_τ s.

Figure 5 depicts the density dependence of the singly-differential cross section from $\rho = 10^{12}$ gm cm $^{-3}$ to $\rho = 3 \times 10^{14}$ gm cm $^{-3}$, with and without many-body effects. The temperature is kept constant at 5 MeV and the incident neutrino energy is 20 MeV. Table III displays the corresponding total suppression factors, $\langle \omega \rangle$, and ω_{rms} . Both Figure 5 and Table III demonstrate that the total suppression effect increases quickly with density beyond 10^{13} gm cm $^{-3}$ and that that due solely to many-body effects increases quickly beyond 10^{14} gm cm $^{-3}$. In fact, the total correlation suppression factor reaches ~ 100 at 10^{15} gm cm $^{-3}$, calling into question the perturbative assumption itself. Nevertheless, it is clear that correlation and many-body effects can drastically lower the neutral-current rates in high-density supernova cores. Note that the widths displayed in Figure 5 increase with increasing ρ . This reflects the increasing nucleon degeneracy and increasing average nucleon energy that accompanies increasing ρ .

Taking a temperature, density and Y_e profile from an early post-bounce model of Burrows, Hayes, & Fryxell [2], we show in Figure 6 the corresponding differential cross section curves at $E_1 = 20$ MeV for a “realistic” profile. Table IV displays the total suppression factors, $\langle \omega \rangle$, and ω_{rms} . The total suppression effect at the center is greater than 30, that due solely to many-body effects is ~ 5 . The $\langle \omega \rangle$ and ω_{rms} are also large. Even at 10^{14} gm cm $^{-3}$, the extra suppression effect due to many-body effects is ~ 2 .

It is interesting to compare the suppression factors calculated from our full equations with those that come from the long-wavelength limits given in eqs. (27) and (29), using the same potential parameters. At a density of 3.0×10^{14} gm cm $^{-3}$, a temperature of 5 MeV, and for neutrino energies less than 10 MeV, the factors, calculated the two different ways, are within 10% of each other. However, for a neutrino energy of 30 MeV, the full calculation gives a suppression that is 30% greater than in the long-wavelength limit. It will be recalled that our “long-wavelength” limit also requires that the energy transfer, ω , be small. Since the energy transfers are of the order of $p_F q$, this limit can be achieved with fixed nucleon mass only by going to lower density. With temperature fixed at 5 MeV, and neutrino energy fixed at 20 MeV, we find less than a 5% discrepancy for a density of 10^{13} gm cm $^{-3}$. However,

the discrepancy rises steadily to nearly 50% at a density of 10^{14} gm cm $^{-3}$. These numbers confirm that the static approach is adequate only in some of parameter realms occupied by supernovae.

C. Correction Factors versus Energy Transfer

It is instructive to calculate $d^2\Gamma/d\omega d\cos\theta$, after integration over $\cos\theta$, (*i.e.*, $d\sigma/d\omega$), with and without the \mathcal{C}_V and \mathcal{C}_A terms and a renormalized nucleon mass, and to take the ratio. This gives one a sense of the integrated correction factor to the differential rate due to many-body effects. This is the many-body correction factor to what might be called $S(\omega)$. Figures 7, 8, 9, and 10 depict the logarithms of these correction factors as a function of ω . These figures correspond to the Figures 3 through 6. We see the expected suppression factor in the small- ω regime that dominates the total suppression integral, but at high $|\omega|$ s we see manifestations of the resonances. The rapid decrease in $\text{Im}\Pi^{(0)}(q, \omega)$ with $|\omega|$ defeats the increase in the correction factor at high $|\omega|$ in the total cross section integral. However, this resonance effect is partly responsible for the high- $|\omega|$ flattening we see in Figures 3 through 6. Note that this correction factor does not go to zero at $\omega = 0$, can go far above 1 for high $|\omega|$ s, and does not have the form, $\omega^2/(\omega^2 + K)$.

VII. AN ILLUSTRATIVE MODEL OF PROTONEUTRON STAR COOLING

While the consequences of the inclusion of many-body effects on neutrino cross sections and energy redistribution are by no means clear, one can straightforwardly ascertain the potential of such effects to alter aspects of supernova and protoneutron star development by performing simplified protoneutron star cooling calculations. We have chosen to investigate the evolution of the electron neutrino luminosity (L_{ν_e}), under certain simplifying assumptions, with and without various ad hoc alterations to the neutrino opacities. The code, developed by Burrows & Lattimer [9], uses the Henyey technique with a simple nuclear EOS, is general-relativistic, and handles the transport of neutrinos of all species in the diffusion approximation. It conserves total energy to about one percent over 20 seconds of evolution. The default cases are models of L_{ν_e} versus time after bounce without accretion and with an assumed accretion rate of $0.4M_{\odot} e^{-t/\tau_a}$, where τ_a is 0.5 seconds. The initial baryon mass is $1.3 M_{\odot}$. We alter the total opacities in an ad hoc fashion to mimic the decreases we can anticipate given our preliminary exploration of neutral-current suppressions and compare the results to the default models. The two exploratory models we present assume that the total opacities are decreased by a fixed amount above a given density, in one case 5×10^{13} gm cm $^{-3}$ and in the other 10^{14} gm cm $^{-3}$. For the 5×10^{13} gm cm $^{-3}$ case the suppressions were 0.3, 0.1, and 0.05 (extreme) and for the 10^{14} gm cm $^{-3}$ case the suppressions were 0.3 and 0.1. These were guided by our results, but should be considered arbitrary. Note that the more conservative case for which the opacity is altered modestly and at the higher density is the more likely.

The results are plotted in Figure 11. From a comparison between the fiducial model and the one without accretion, one notes that accretion dominates as a power source in the early seconds. If the supernova is reignited within the first hundreds of milliseconds, it is

unlikely that the new opacities at high densities will play a central role in its revitalization. However, if the delay to explosion is many hundreds of milliseconds to seconds, higher L_{ν_e} s occasioned by the many-body and final-state nucleon blocking effects may well play a role in the supernova, and in powering the explosion after it is relaunched. Even partially enhanced luminosities have been shown to be important for neutrino-driven explosions [2,5,42,43]. As Figure 11 demonstrates, the lower the density at which opacities are altered, the earlier the effect. The enhancements in the luminosities after a few seconds can be a factor of two, though enhancements of 30%–50% are more likely. Since energy is conserved, the luminosities at later times (5–60 seconds, not shown) are decreased relative to the those of the fiducial model. Within this model set, the theoretical signals in Kamioka II [6] and IMB [7] range by no more than a factor of two. Drastic decreases in the total opacities translate into only moderate (but intriguing) changes in L_{ν_e} and the signals because even a completely transparent core merely flattens the interior temperature gradients. The energy must still diffuse through the unaltered density region below 5×10^{13} or 10^{14} gm cm⁻³.

We point out that for progenitor stars in the $8 M_{\odot}$ to $13 M_{\odot}$ mass range early accretion onto the protoneutron star before explosion will be slight. Hence, alterations in the high-density neutrino cross sections might show themselves earlier in lower-mass progenitors, in time to be more unambiguously of importance in reigniting and powering the supernova. Nevertheless, the reader should be cautioned that these conclusions await a more thoughtful implementation of these new neutrino opacities and that the calculations depicted in Figure 11 are merely suggestive.

VIII. CONCLUSIONS

In this paper, we have developed a consistent formalism for calculating the Fermi and Gamow–Teller structure functions in nuclear matter, including many-body correlations and the full kinematics of neutrino–nucleon scattering. Previously all but ignored, the effects of density–density and spin–spin correlations on neutrino scattering rates are found to be significant. Above nuclear density, the total cross section suppression factor due to final-state nucleon blocking, correlations, and a reduction in the nucleon effective mass can be more than an order of magnitude. The upshot is that supernova cores are more transparent than previously thought. Since the many-body corrections to the charged-current rates for the ν_e s have yet to be published, in this paper we conclude only that the total opacities of nuclear matter to ν_{μ} s and ν_{τ} s (and their anti-particles) are qualitatively altered. The magnitude of the rate corrections due to many-body effects increases with density, decreases with temperature, and is roughly independent of incident neutrino energy.

In addition, we find that the neutrino–matter energy transfer rates due to neutrino–nucleon scattering are much larger than heretofore assumed. As a consequence, energy equilibration for the non-electron-type neutrino species may well be by what was previously considered an elastic process. This obtains even for free nucleons at high densities, but is all the more true with many-body effects included. An identifiable part of the energy transfer enhancement comes from the excitation of collective modes in the matter, modes akin to the Gamow–Teller and Giant Dipole resonances in nuclei. Energy is transferred by the Čerenkov mechanism to or from these modes when the energy transfer ($\pm\omega$) and momentum transfer (q) satisfy the dispersion relation of the medium’s excitations (zero sound and spin sound,

both of which require repulsive interactions).

Under the assumption that both the charged-current and the neutral-current cross sections are decreased, we calculated a set of ad hoc protoneutron star cooling models to gauge the importance of the new opacities to the supernova itself. While the early luminosities are not altered, the luminosities after many hundreds of milliseconds to seconds can be altered by factors that range from 10% to 100%. Such factors may have a bearing on the efficacy of the neutrino-driven supernova mechanism, the delay to explosion, the energy of the explosion, and the strength and relative role of convective overturn. The magnitude of the relative enhancement of the driving luminosity is a function of the post-bounce mass accretion rates and may be larger for the least massive, massive stars. Hence, these new opacities may be more germane to the terminal behavior of the massive stars most favored by the IMF.

It remains to derive the effects of correlations on the charged-current rates, as well as to develop a simple algorithm for incorporating these effects into supernova and protoneutron star codes, with full energy redistribution. Since many-body effects at the highest densities are quite large, a non-perturbative approach may need to be developed for the deep interiors. Furthermore, the structure function calculations should be done in a manner fully consistent with the equation of state employed, since the physics of the two are inextricably linked.

If we find that there is indeed an across-the-board reduction in the neutrino-matter rates at high densities, it will be yet another reminder that the keys to the supernova puzzle and its systematics lie not in any one realm of expertise (radiative transfer, hydrodynamics, the equation of state, the weak interaction, etc.), but in all, and that the 20% effects we seek under lamp posts might at times divert us from discovering those far larger just a few steps down the street.

ACKNOWLEDGMENTS

We would like to acknowledge stimulating and productive conversations with S. Reddy, M. Prakash, G. Raffelt, D. Seckel, and J. Lattimer, as well as support from the NSF under grant No. AST-96-17494. We would also like to acknowledge the germinating influence of the Santa Barbara Institute for Theoretical Physics, supported by the NSF under grant No. PHY94-07194.

APPENDIX A

To get expressions for the real and imaginary parts of $\Pi^{(0)}$ that are efficient for computation, we begin with FW (33.4), with notations changed to those of this paper

$$\Pi^{(0)}(q, \omega) = -2 \int \frac{d^3p}{(2\pi)^3} \frac{f_{\mathbf{p}+\mathbf{q}} - f_{\mathbf{p}}}{\omega + i\eta + \epsilon_{\mathbf{p}} - \epsilon_{\mathbf{p}+\mathbf{q}}}. \quad (55)$$

We can write each of the Fermi-Dirac distributions that appear here as a sum of Boltzmann distributions,

$$f(\mathbf{p}) = \sum_{j=1}^{\infty} (-1)^{j+1} e^{j\beta(\mu - \epsilon_{\mathbf{p}})}. \quad (56)$$

We use this expansion, together with FW (33.8) for the imaginary part of $\Pi^{(0)}$ in the Boltzmann limit, to obtain,

$$\text{Im}\Pi^{(0)}(q, \omega) = \frac{m^2}{2\pi\beta q} \sum_{j=1}^{\infty} (-1)^{j+1} j^{-1} \left[e^{j(\beta\mu - Q^2)} - e^{j(\beta\mu - Q^2 - \beta\omega)} \right], \quad (57)$$

where

$$Q = \left(\frac{m\beta}{2}\right)^{1/2} \left(-\frac{\omega}{q} + \frac{q}{2m}\right) \quad (58)$$

and the terms with $j > 1$ in the series come from the replacement, $\beta \rightarrow j\beta$, in the Boltzmann result. The sum is easily performed to give the result shown in (36). For the real part, we use the same trick, beginning with the Boltzmann form (FW 33.9),

$$\text{Re}\Pi^{(0)}(q, \omega)_{\text{boltz}} = \frac{m^2}{2\pi^{3/2}\beta q} e^{-\beta\mu} \Phi(Q) + (\omega \rightarrow -\omega), \quad (59)$$

where

$$\Phi(Q) = 2Q \int_0^1 dy e^{Q^2(y^2-1)}. \quad (60)$$

We obtain,

$$\text{Re}\Pi^{(0)}(q, \omega) = \frac{m^2}{2\pi^{3/2}\beta q} Q \int_0^1 dy \sum_{j=1}^{\infty} (-1)^{j+1} j^{-1/2} e^{j(\beta\mu + Q^2(y^2-1))} + (\omega \rightarrow -\omega). \quad (61)$$

Next, we represent the $j^{-1/2}$ factor under the sum by $\pi^{-1/2} \int_{-\infty}^{\infty} ds e^{-js^2}$, so that we can sum the geometric series. Displacing the s integration variable $s \rightarrow s + QY$, we obtain,

$$\text{Re}\Pi^{(0)}(q, \omega) = \frac{m^2}{\pi^2\beta q} Q \int_{-\infty}^{\infty} ds \int_0^1 dy \frac{e^{-(s^2+2sQy+Q^2+\beta\mu)}}{1 + e^{-(s^2+2sQy+Q^2+\beta\mu)}} + (\omega \rightarrow -\omega). \quad (62)$$

The y integral is now easily performed to give the result (35).

APPENDIX B

We show directly that in the large- m , small- q limits the complete correlation functions as calculated in the ring sum in §IV reduce to the long-wavelength limits that were determined from the single-particle energies in §II. In the large- m limit, the function $\text{Im}\Pi^{(0)}(q, \omega)$ becomes more and more concentrated around $\omega = 0$, so that to calculate the rate we set ω equal to zero, except in the factor,

$$I_1 = \pi^{-1} \int_{-\infty}^{\infty} d\omega \text{Im}\Pi(q, \omega) (1 - e^{-\beta\omega})^{-1}. \quad (63)$$

In the limit, we make the replacement $(1 - e^{-\beta\omega}) \rightarrow \beta\omega$ and use the Kramers-Kronig dispersion relation in the variable ω to write $I_1 \rightarrow \text{Re}\Pi(q, \omega = 0)$. Finally, we use (35) in the limit $Q \rightarrow 0$ to show that $\text{Re}\Pi^{(0)}(0, 0) = -h(\mu)$, where $h(\mu)$ is the function defined in (13). The ring approximation for the one-channel case (34) with a potential U now reads,

$$I_1 \rightarrow h(\mu)/(1 + Uh(\mu)), \quad (64)$$

in agreement with (14).

TABLES

TABLE I. The total suppression factors (\mathcal{S}), average energy transfers ($\langle\omega\rangle$) and *rms* energy transfers (ω_{rms}) for various incident neutrino energies (E_1). The temperature is 5 MeV, the density is 3×10^{14} gm cm⁻³, and the electron fraction is 0.3. These quantities are shown for both the many-body case and for the case without correlations or a renormalized mass (subscript or superscript 0). All the energies are in MeV. For the many-body case, the default nuclear model described in the text is employed. The suppression factors are the factors by which the default total cross section should be multiplied to obtain the corrected total cross section.

E_1 (MeV)	\mathcal{S}	\mathcal{S}_0	$\langle\omega\rangle$ (MeV)	$\langle\omega\rangle_0$ (MeV)	ω_{rms} (MeV)	ω_{rms}^0 (MeV)
1	0.131	0.217	-0.917	-0.207	0.592	0.295
5	0.090	0.202	-3.749	-0.852	3.088	1.432
10	0.060	0.186	-5.064	-3.000	6.068	2.755
15	0.045	0.173	-4.204	-1.288	8.241	3.939
20	0.038	0.164	-2.156	-0.970	9.492	4.977
25	0.035	0.158	0.287	-0.385	10.195	5.881
30	0.034	0.154	2.779	0.402	10.687	6.671
40	0.035	0.152	7.583	2.375	11.569	8.007
50	0.038	0.155	12.109	4.649	12.522	9.143
60	0.041	0.161	16.413	7.063	13.574	10.177
70	0.046	0.169	20.549	9.532	14.712	11.161

TABLE II. As in Table I, the total suppression factors (\mathcal{S}), average energy transfers ($\langle\omega\rangle$) and *rms* energy transfers (ω_{rms}), but for various temperatures at a given incident neutrino energy ($E_1 = 20$ MeV). The 0 subscript or superscript corresponds to the case without many-body effects, but with final-state nucleon blocking. This table corresponds to Figure 4, but also includes numbers for $T = 3$ MeV.

T (MeV)	\mathcal{S}	\mathcal{S}_0	$\langle\omega\rangle$ (MeV)	$\langle\omega\rangle_0$ (MeV)	ω_{rms} (MeV)	ω_{rms}^0 (MeV)
3	0.021	0.093	2.693	0.598	6.623	4.292
5	0.038	0.164	-2.158	-0.970	9.497	4.977
7	0.065	0.240	-6.153	-1.856	11.221	5.358
10	0.118	0.350	-10.193	-2.699	12.482	5.810
15	0.227	0.516	-14.355	-3.734	13.928	6.614
20	0.351	0.659	-17.572	-4.726	15.695	7.618
30	0.639	0.900	-24.603	-7.118	21.660	10.575

TABLE III. As in Tables I & II, the total suppression factors (\mathcal{S}), average energy transfers ($\langle \omega \rangle$) and *rms* energy transfers (ω_{rms}), but for various mass densities (ρ) at a given incident neutrino energy ($E_1 = 20$ MeV) and for a temperature of 5 MeV. The 0 subscript or superscript corresponds to the case without many-body effects, but with final-state nucleon blocking. This table is related to Figure 5.

ρ (gm cm ⁻³)	\mathcal{S}	\mathcal{S}_0	$\langle \omega \rangle$ (MeV)	$\langle \omega \rangle_0$ (MeV)	ω_{rms} (MeV)	ω_{rms}^0 (MeV)
10 ¹²	0.897	0.952	-0.295	0.216	2.556	2.157
10 ¹³	0.560	0.794	-0.455	0.256	3.211	2.359
3 × 10 ¹³	0.307	0.591	-0.766	-0.337	4.269	2.725
10 ¹⁴	0.117	0.162	-1.525	-0.562	6.532	3.598
3 × 10 ¹⁴	0.038	0.164	-2.156	-0.970	9.492	4.977

TABLE IV. As in the other tables, the total suppression factors (\mathcal{S}), average energy transfers ($\langle \omega \rangle$) and *rms* energy transfers (ω_{rms}), but for a post-bounce profile from Burrows, Hayes, & Fryxell (1995), at a given incident neutrino energy ($E_1 = 20$ MeV). The 0 subscript or superscript corresponds to the case without many-body effects, but with final-state nucleon blocking. This table is related to Figure 6. The density and temperature at the edited points in the model are indicated.

ρ (gm cm ⁻³)	T (MeV)	\mathcal{S}	\mathcal{S}_0	$\langle \omega \rangle$ (MeV)	$\langle \omega \rangle_0$ (MeV)	ω_{rms} (MeV)	ω_{rms}^0 (MeV)
3.945 × 10 ¹⁴	5.053	0.028	0.136	-2.142	-1.136	10.082	5.426
3.084 × 10 ¹⁴	5.518	0.043	0.180	-3.305	-1.261	10.135	5.137
2.049 × 10 ¹⁴	9.457	0.147	0.402	-7.322	-2.108	10.290	5.130
1.281 × 10 ¹⁴	10.561	0.243	0.547	-5.797	-1.882	8.656	4.706
6.463 × 10 ¹³	13.531	0.477	0.792	-4.629	-1.946	7.460	4.659
4.322 × 10 ¹³	14.554	0.608	0.880	-4.065	-1.959	6.994	4.666
2.669 × 10 ¹³	15.611	0.750	0.953	-3.660	-2.013	6.676	4.735
5.972 × 10 ¹²	11.287	0.876	0.968	-1.740	-1.159	4.554	3.609
1.082 × 10 ¹²	6.137	0.907	0.957	-0.509	-0.369	2.874	2.416

REFERENCES

- [1] H.A. Bethe & J.R. Wilson, *Astrophys. J.* **295**, 14 (1985).
- [2] A. Burrows, J. Hayes, & B.A. Fryxell, *Astrophys. J.* **450**, 830 (1995).
- [3] M. Herant, W. Benz, R. Hix, C. Fryer, & S.A. Colgate, *Astrophys. J.* **435**, 339 (1994).
- [4] H.-T. Janka & E. Müller, *Astron. and Astrophys.* **306**, 167 (1996).
- [5] R. Mayle & J.R. Wilson, *Astrophys. J.* **334**, 909 (1988).
- [6] K. Hirata, *et al.*, *Phys. Rev. Lett.*, **58**, 1490 (1987).
- [7] R. M. Bionta, *et al.*, *Phys. Rev. Lett.* **58**, 1494 (1987).
- [8] A. Burrows, *Astrophys. J.* **334**, 891 (1988).
- [9] A. Burrows & J. M. Lattimer, *Astrophys. J.* **307**, 178 (1986).
- [10] T.A. Weaver & S.E. Woosley, *Astrophys. J. Suppl.* **101**, 181 (1995).
- [11] F.X. Timmes, S.E. Woosley, & T.A. Weaver, *Astrophys. J.* **457**, 854 (1996).
- [12] A. Burrows & J. Hayes, *Phys. Rev. Letters* **76**, 352 (1996).
- [13] D. Wooden, to be published in the proceedings of the 5'th CTIO/ESO/LCO Workshop entitled "SN1987A: Ten Years Later," eds. M.M. Phillips & N.B. Suntzeff, held in La Serena, Chile, February 24-28, 1997.
- [14] I. Lichtenstadt, A. Khokhlov, & J.C. Wheeler, in preparation (1997).
- [15] A. Mezzacappa, A.C. Calder, S.W. Bruenn, J.M. Blondin, M.W. Guidry, M.R. Strayer, & A.S. Umar, *Astrophys. J.*, in press (1998).
- [16] D. L. Tubbs & D. N. Schramm, *Astrophys. J.* **201**, 467 (1975).
- [17] S. L. Glashow, *Nucl. Phys.* **22**, 579 (1961).
- [18] S. Weinberg, *Phys. Rev. Lett.* **19**, 1264 (1967).
- [19] C. J. Horowitz & K. Wehrberger, *Nucl. Phys.* **A531**, 665 (1991); *Phys. Rev. Lett.* **66**, 272 (1991); *Phys. Lett.* **B226**, 236 (1992).
- [20] A. Mezzacappa & S.W. Bruenn, *Astrophys. J.*, in press (1997).
- [21] N. Iwamoto & C. J. Pethick, *Phys. Rev.* **D25**, 313 (1982).
- [22] B. T. Goodwin & C. J. Pethick, *Astrophys. J.* **253**, 816 (1982).
- [23] W. Keil, H-T. Janka & G. Raffelt, *Phys. Rev.* **D51**, 6635 (1995).
- [24] H-T. Janka, W. Keil, G. Raffelt, & D. Seckel, *Phys. Rev. Lett.* **76**, 2621 (1996).
- [25] G. Sigl, *Phys. Rev. Lett.* **76**, 2625 (1996).
- [26] S. W. Bruenn, *Astrophys. J. Suppl.* **58**, 771 (1985).
- [27] P. J. Schinder, *Astrophys. J. Suppl.* **74**, 249 (1990).
- [28] D. Q. Lamb & C. J. Pethick, *Astrophys. J.* **209**, L77 (1976).
- [29] S. Hannestad & G. Raffelt, *Phys. Rev.* **D**, submitted (1997).
- [30] S. Reddy, M. Prakash, & J.M. Lattimer, *Phys. Rev.* **D**, in press (1998).
- [31] S. Reddy & M. Prakash, in *Proc. 11th Winter Workshop on Nuclear Dynamics, Advances in Nuclear Dynamics*, ed. W. Bauer and Migerney (New York: Plenum), p. 237 (1995).
- [32] S. Reddy & M. Prakash, *Astrophys. J.* **423**, 689 (1997).
- [33] L.D. Landau and E.M. Lifschitz, *Statistical Physics*, 2'nd edition (Pergamon Press; New York) p.352 (1969); Eqs. (114.13) and (114.14)
- [34] R. F. Sawyer, *Phys. Rev.* **C40**, 865 (1989).
- [35] A.L. Fetter & J.D. Walecka, *Quantum Theory of Many Particle Systems* (New York: McGraw-Hill), 1971.
- [36] B. Friedman & V.R. Pandharipande, *Nucl. Phys.* **A361**,501 (1981).

- [37] R. Schiavilla, V. R. Pandharipande, & R. B. Wiringa, *Nuc. Phys.* **A449**, 219 (1986).
- [38] S.-O. Backman, G. E. Brown, & J. A. Niskanen, *Physics Reports*, **124**, 1 (1985).
- [39] G.E. Brown & M. Rho , *Nucl. Phys.* **A 372**, 397 (1981).
- [40] A. Mezzacappa & S. W. Bruenn, *Astrophys. J.* **405**, 637 (1993).
- [41] D. L. Tubbs, *Astrophys. J. Suppl.* **37**, 287 (1978).
- [42] H.-T. Janka, in the *7th Workshop on Nuclear Astrophysics*, eds. W. Hillebrandt and E. Müller (Max-Planck-Institut für Astrophysik), p. 18 (1993).
- [43] A. Burrows & J. Goshy *Astrophys J.* **416**, L75 (1993).

FIGURES

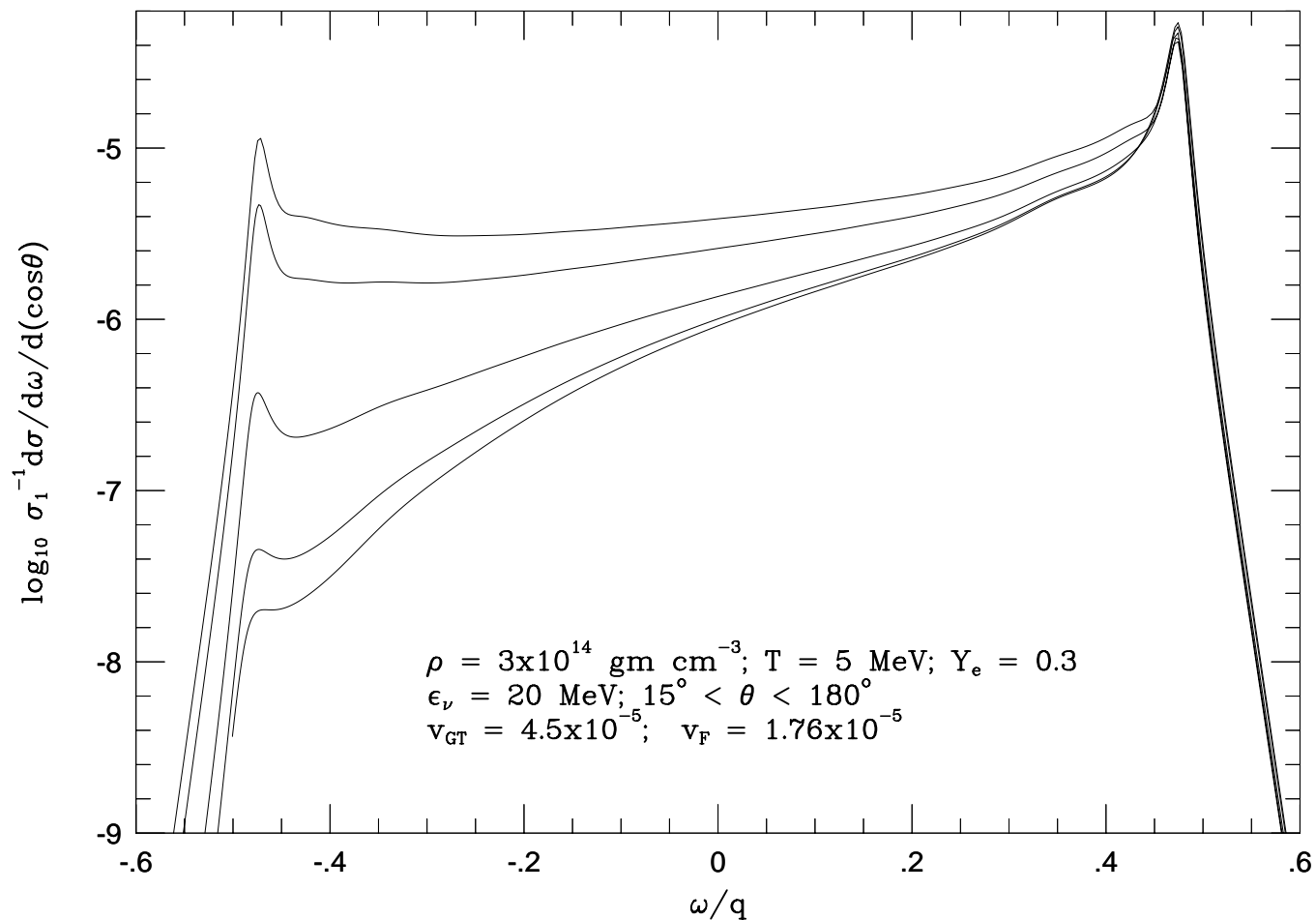


FIG. 1. \log_{10} of the doubly-differential cross section for neutral-current neutrino-nucleon scattering versus ω/q for scattering angles 15° , 45° , 90° , 135° , and 180° . The calculations were performed at a temperature of 5 MeV, a Y_e of 0.3, a ρ of $3 \times 10^{14} \text{ gm cm}^{-3}$, and an incident neutrino energy of 20 MeV. The default potentials ($v_{GT} = 4.5 \times 10^{-5}$ and $v_F = 1.76 \times 10^{-5}$) and effective mass ($m^* = 0.75 m_n$) were employed. The differential cross section is divided by the total scattering cross section (σ_1) in the non-interacting, no-nucleon-blocking, $\omega = 0$ limit.

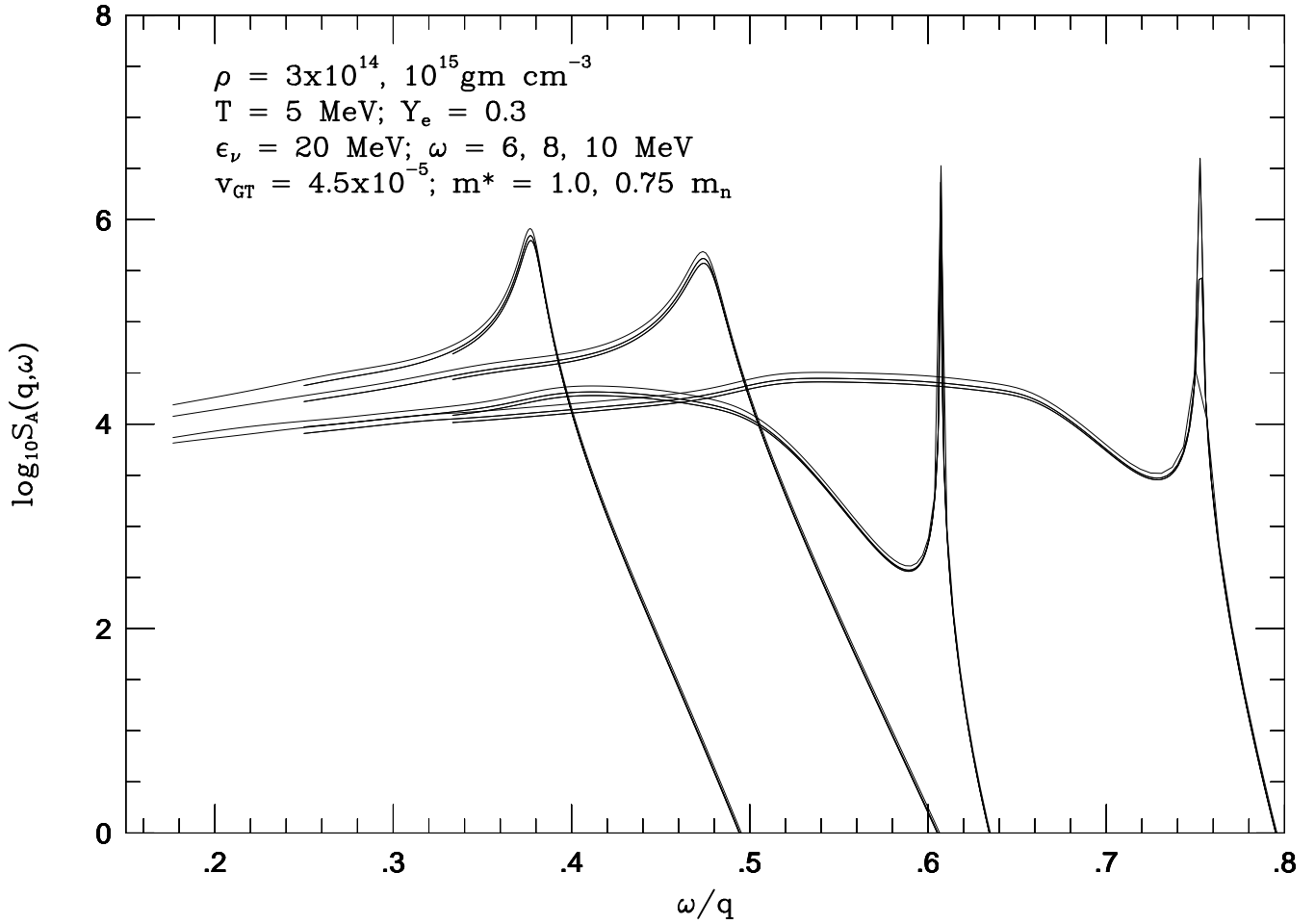


FIG. 2. \log_{10} of the Gamow–Teller structure function versus ω/q for an incident neutrino energy of 20 MeV, energy transfers, ω , of 6, 8, and 10 MeV, two values of the effective mass ($m^* = [0.75m_n, 1.0m_n]$) and two values of the density ($\rho = 3 \times 10^{14}$ and 10^{15} gm cm^{-3}). A temperature of 5 MeV and a Y_e of 0.3 were used, as was the default v_{GT} ($= 4.5 \times 10^{-5}$).

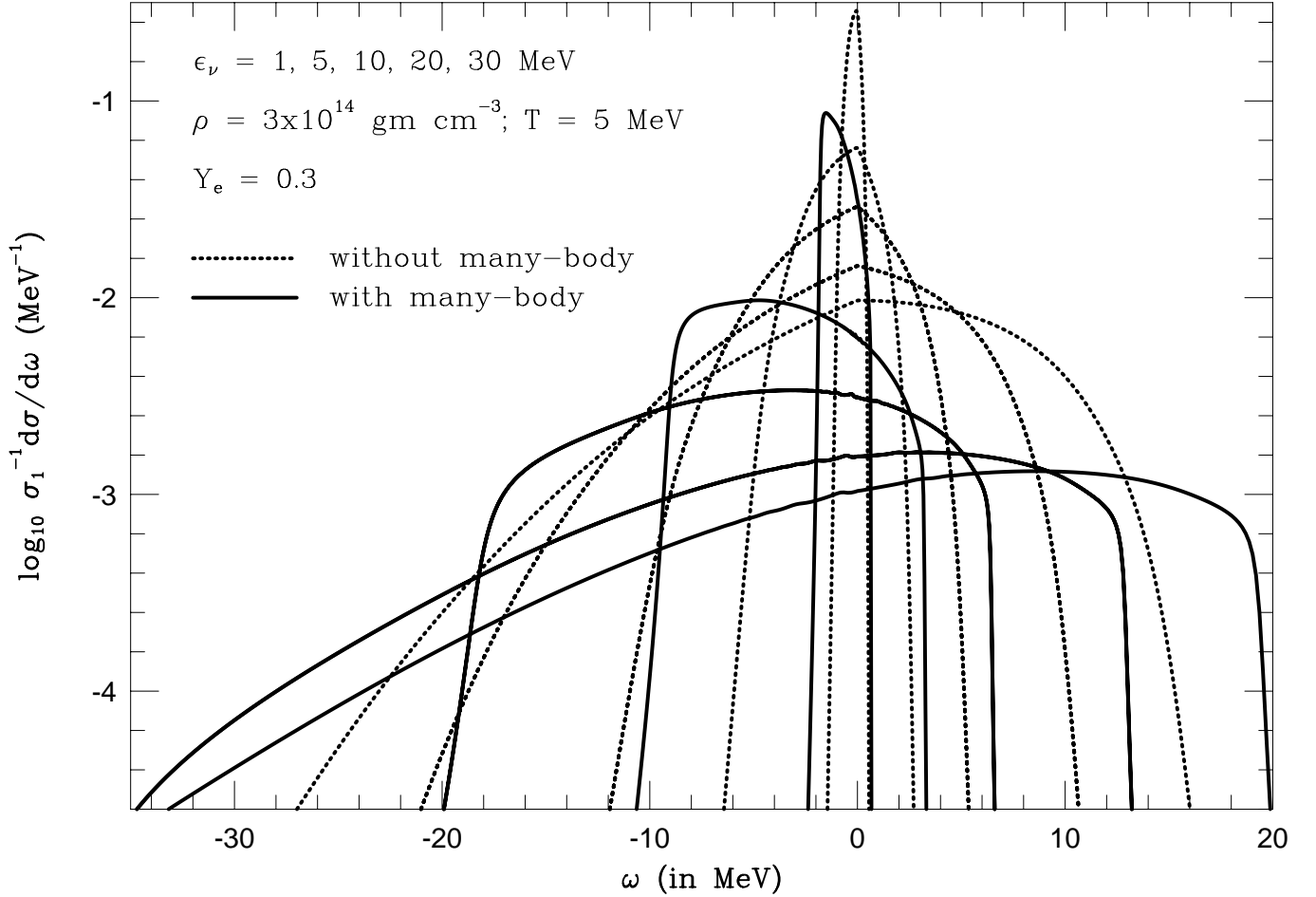


FIG. 3. The \log_{10} of the differential cross section for ν -nucleon scattering versus the energy transfer, ω , for various values of the incident neutrino energy ($\epsilon_\nu = 1, 5, 10, 20, 30$ MeV). The dashed curves neglect the many-body effects associated with m^* and $\mathcal{C}_{\nu,\mathcal{A}}$, while the solid curves include them. A density of 3×10^{14} gm cm $^{-3}$, a temperature of 5 MeV, and an electron fraction, Y_e , of 0.3 were assumed. The curves were normalized to the total ν -nucleon scattering cross section without nucleon blocking or many-body effects.

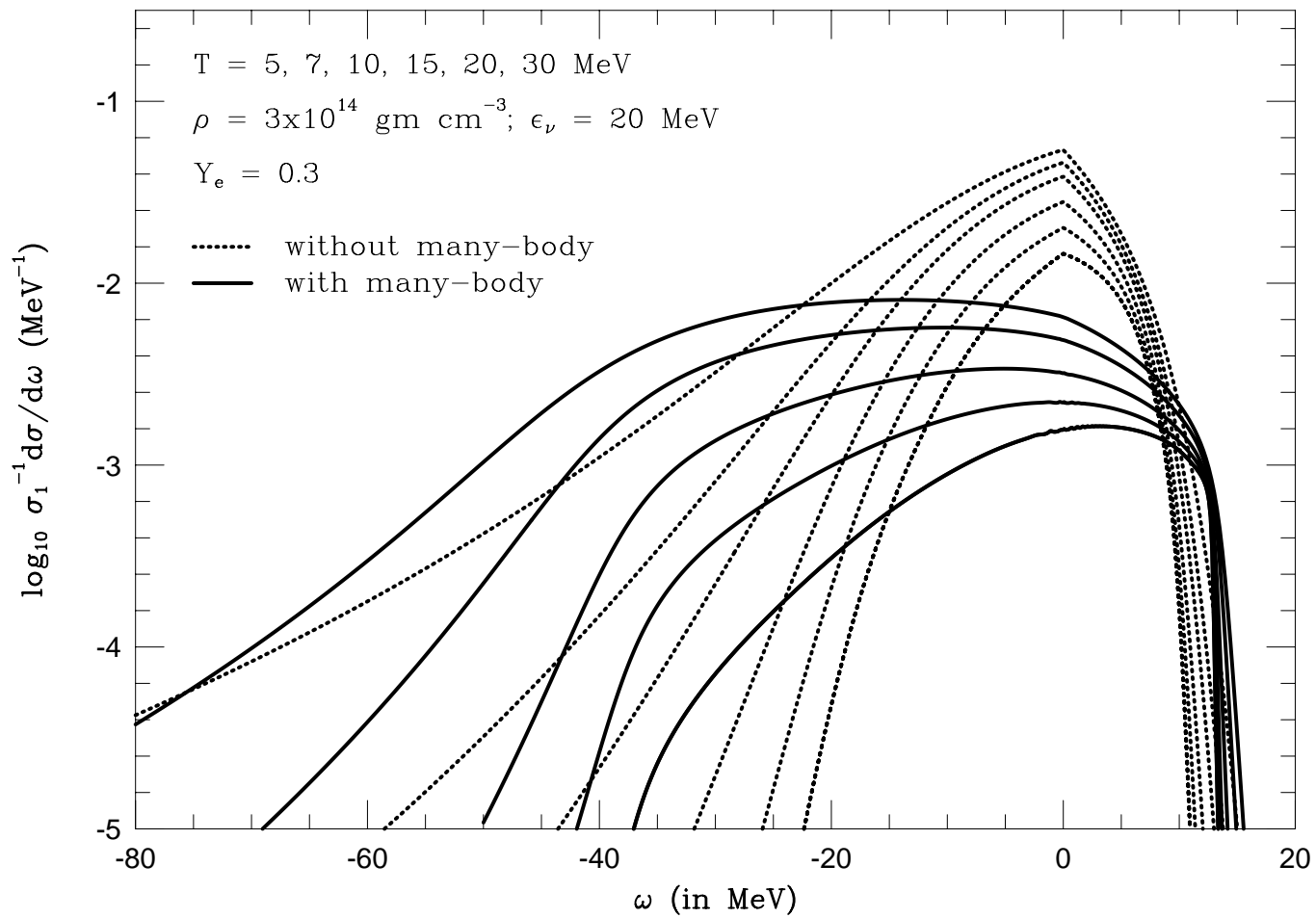


FIG. 4. Similar to Figure 3, but for various temperatures (5, 7, 10, 15, 20, 30 MeV) and at an incident neutrino energy of 20 MeV.

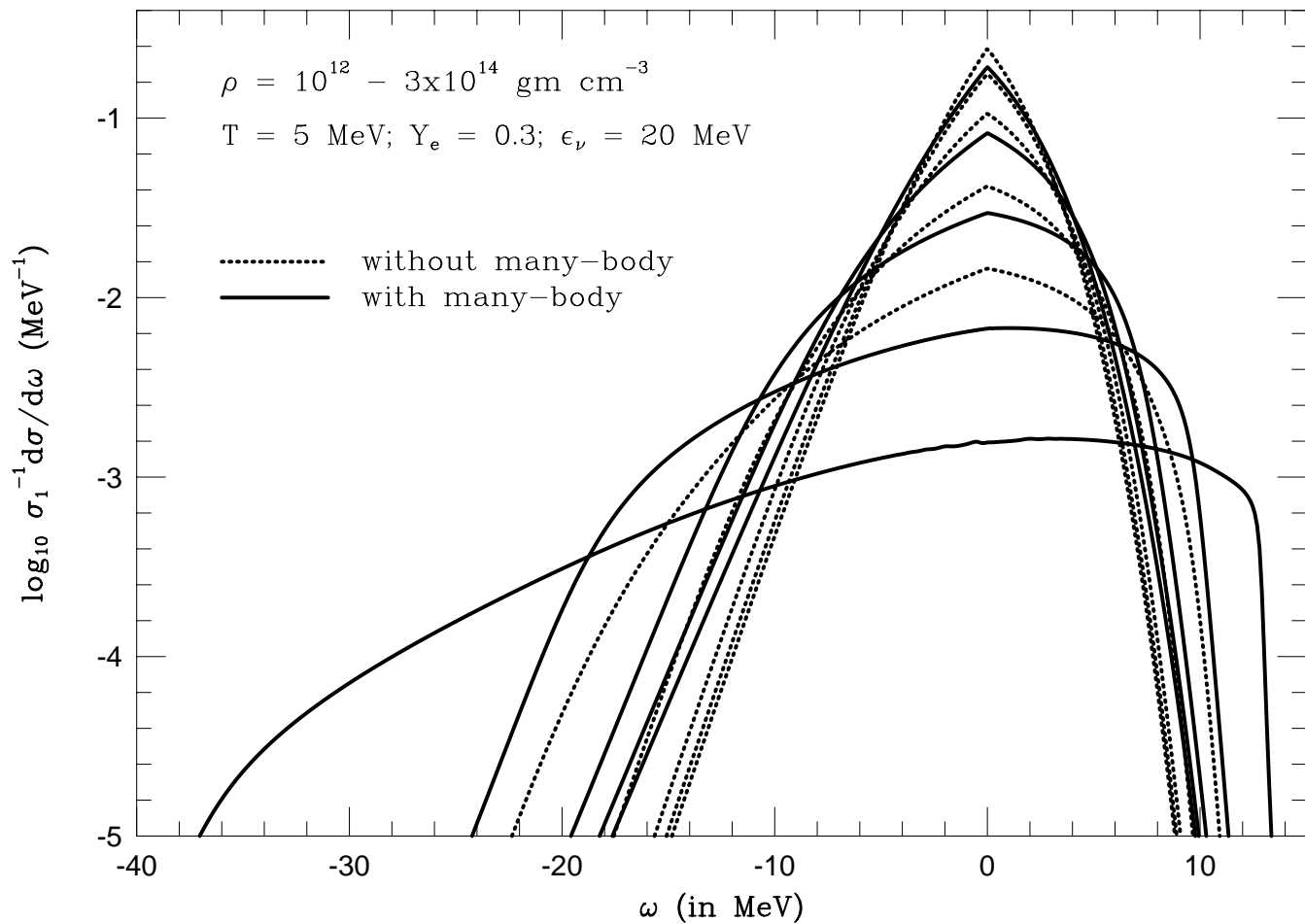


FIG. 5. Similar to Figure 3, but for various densities (10^{12} , 10^{13} , 3×10^{13} , 10^{14} , and 3×10^{14} gm cm^{-3}), a temperature of 5 MeV, and an incident neutrino energy of 20 MeV.

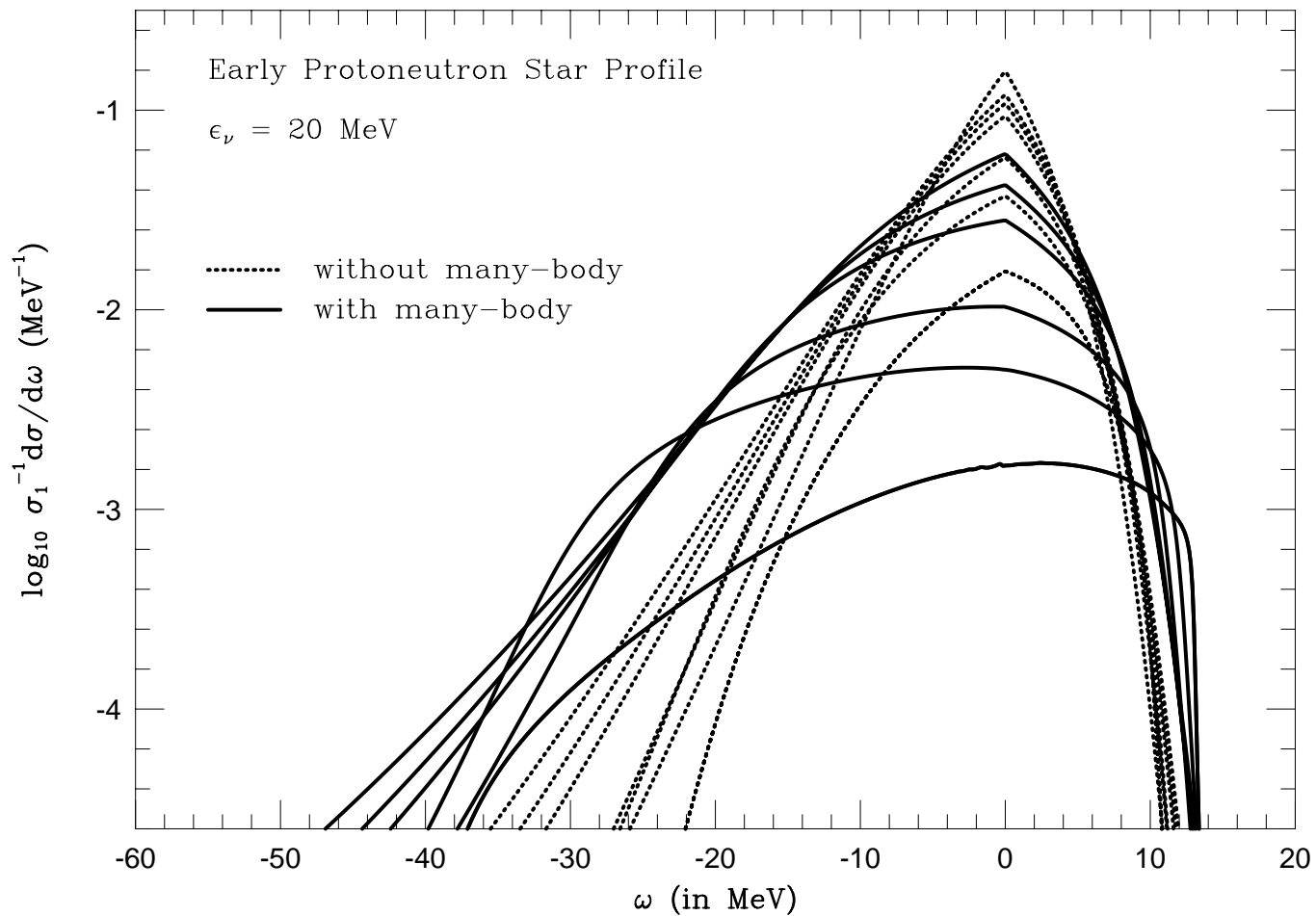


FIG. 6. Similar to Figure 3, but for an early post-bounce temperature-density- Y_e profile from Burrows, Hayes, & Fryxell (1995) (see Table IV). The incident neutrino energy was assumed to be 20 MeV.

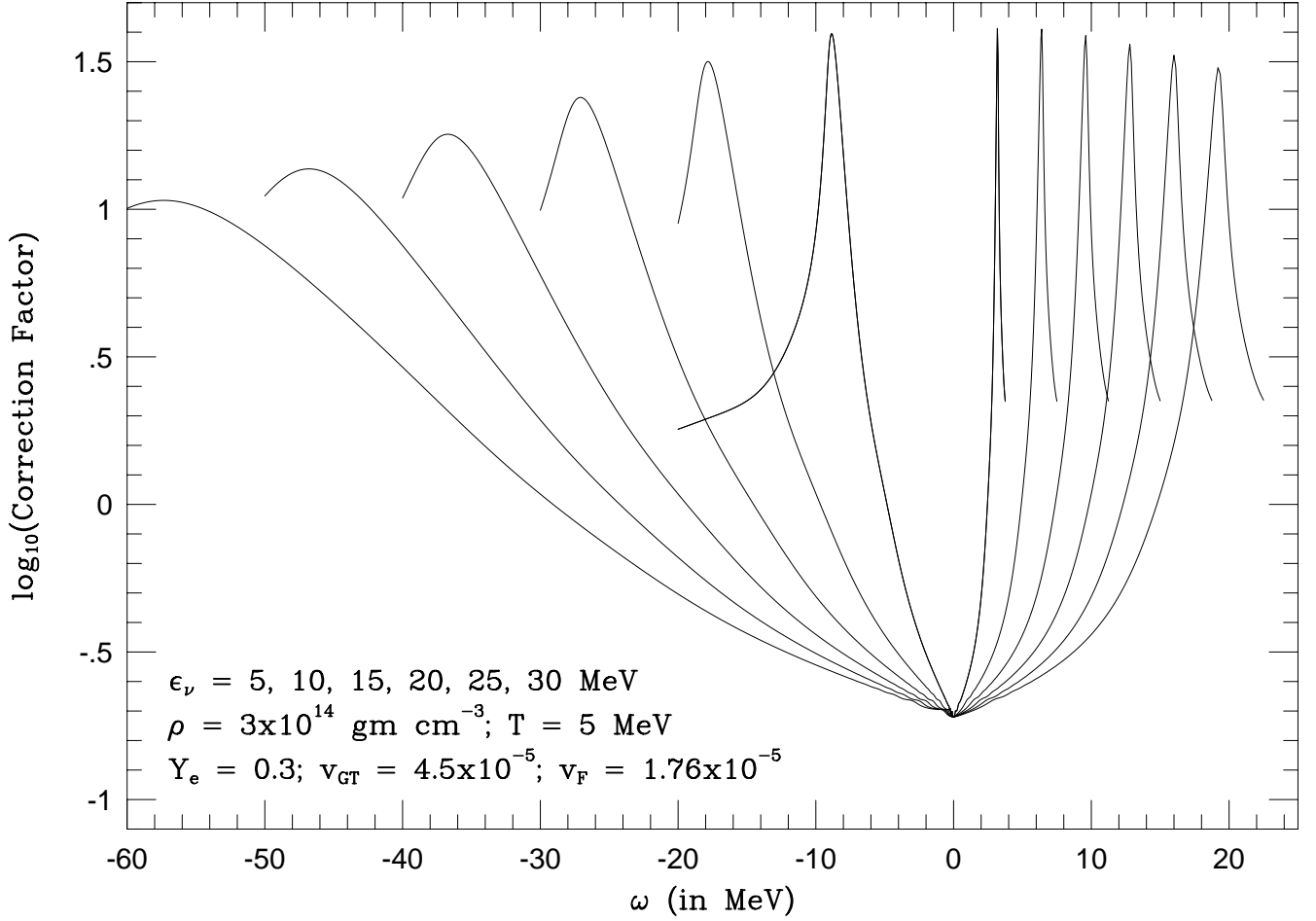


FIG. 7. \log_{10} of the correction factor due to both $\mathcal{C}_{\nu, A}$ and an effective mass of $0.75m_n$ that corresponds to Figure 3 (the $\epsilon_\nu = 1 \text{ MeV}$ line has been omitted). There is suppression at low $|\omega|$ s, but a resonant enhancement at high $|\omega|$ s. Note that at very small $|\omega|$ s the factor is a weak function of incident neutrino energy.

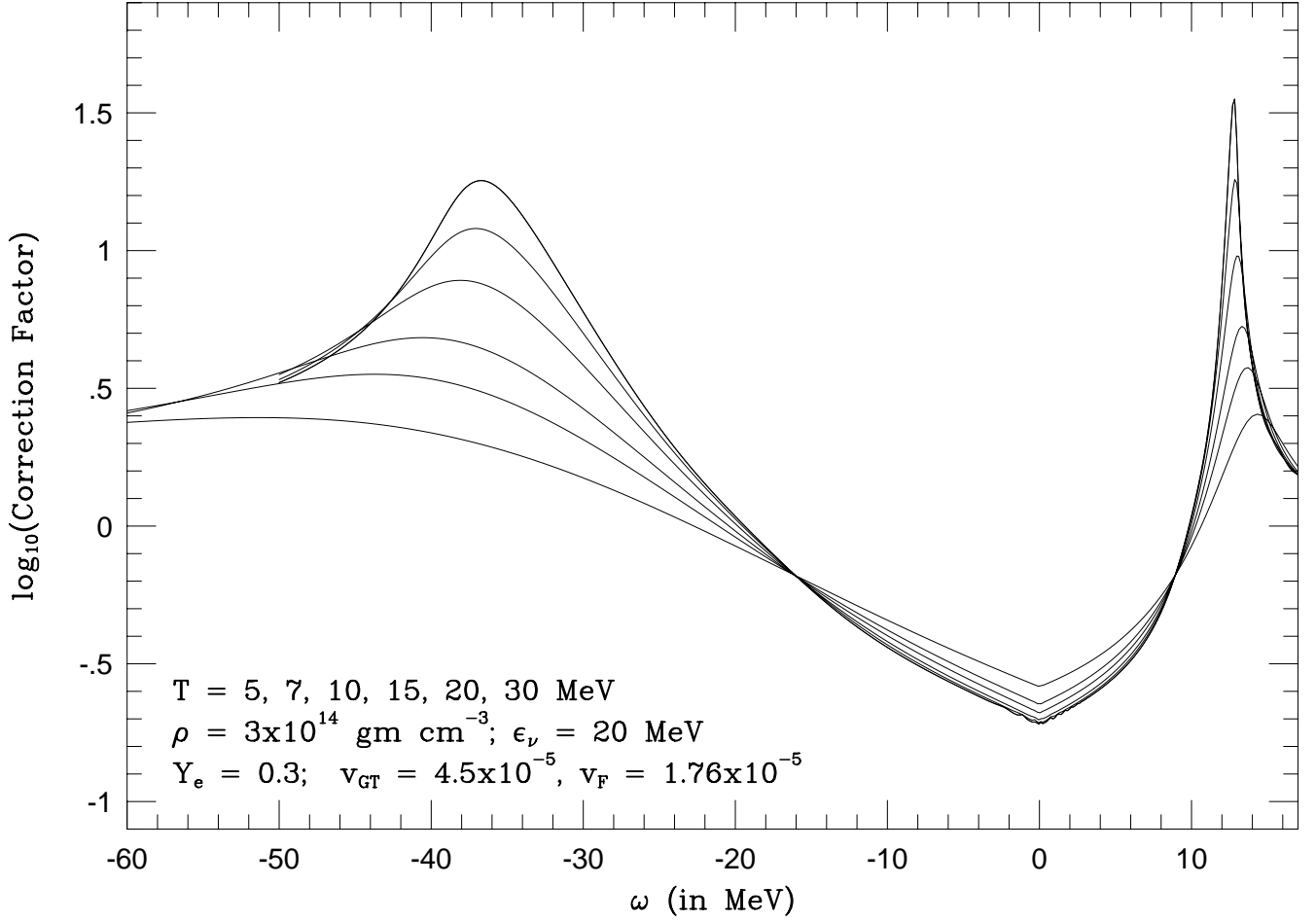


FIG. 8. \log_{10} of the correction factor due to both $\mathcal{C}_{\nu, \mathcal{A}}$ and an effective mass of $0.75m_n$ that corresponds to Figure 4. There is suppression at low $|\omega|$ s, but a resonant enhancement at high $|\omega|$ s. Note that at small $|\omega|$ s the magnitude of the correction is a decreasing function of temperature.

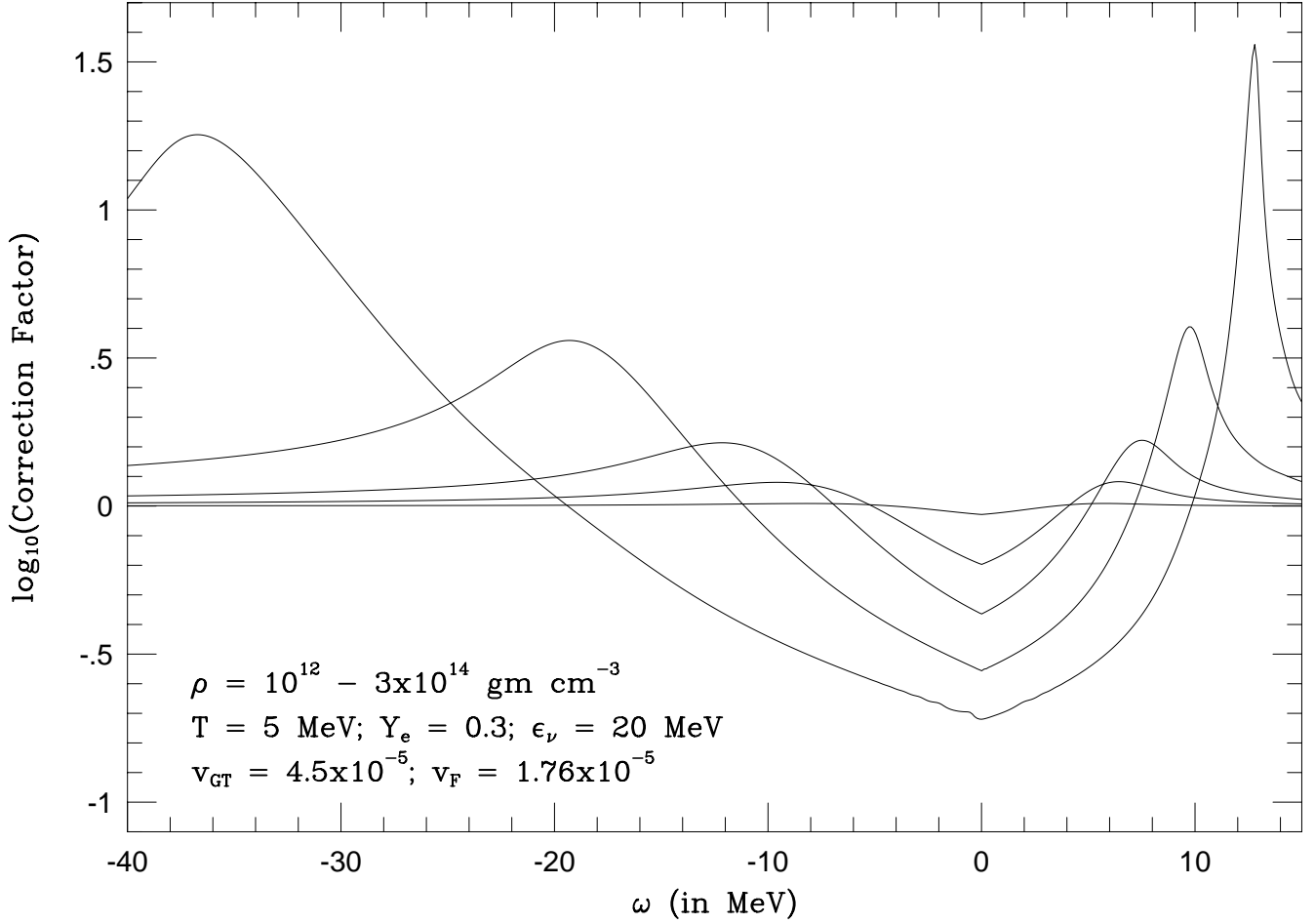


FIG. 9. \log_{10} of the correction factor due to both $\mathcal{C}_{\nu, A}$ and an effective mass of $0.75m_n$ that corresponds to Figure 5. There is suppression at low $|\omega|$ s, but a resonant enhancement at high $|\omega|$ s. Note that at small $|\omega|$ s the factor is a strong function of density.

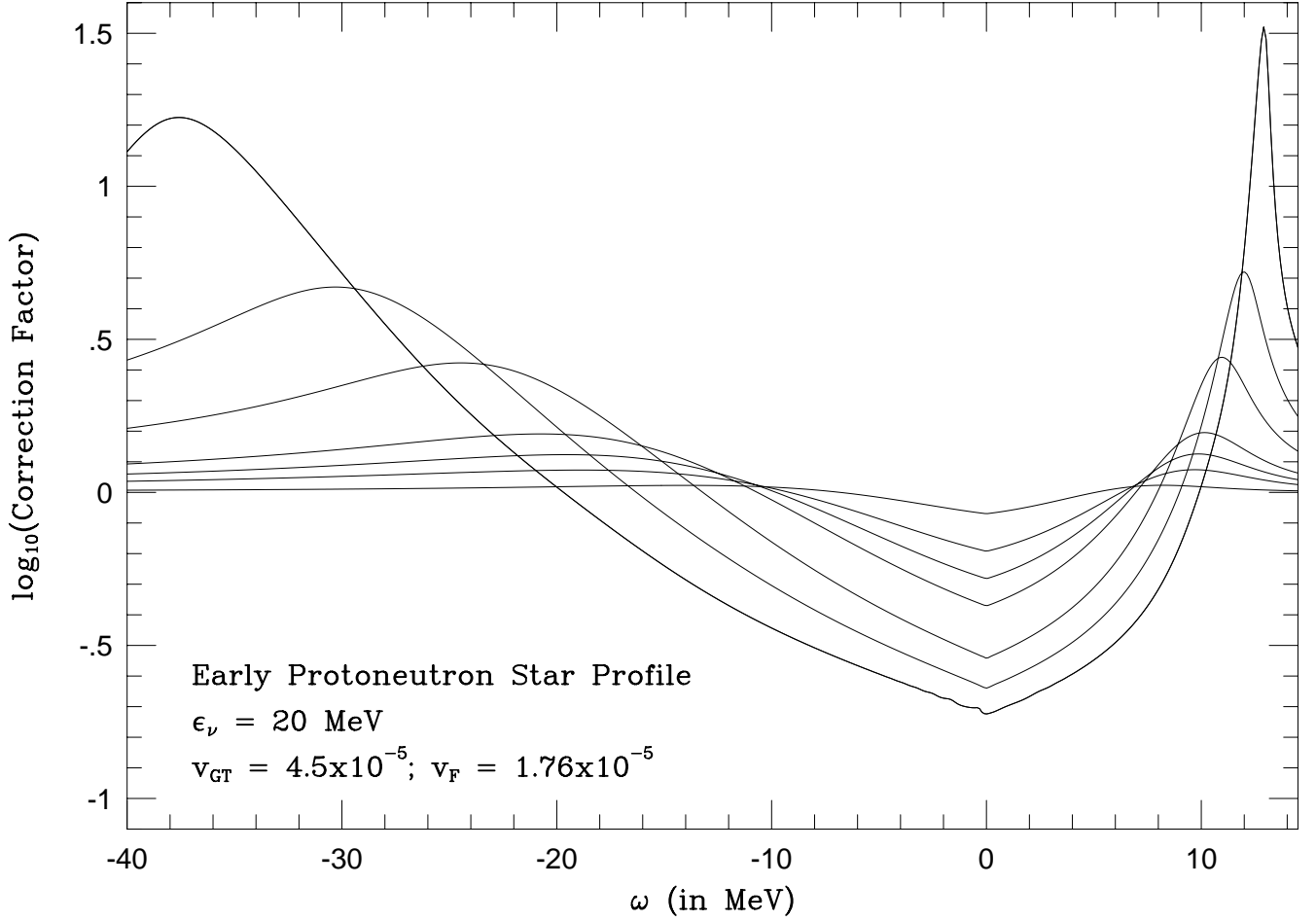


FIG. 10. Log_{10} of the correction factor due to both $\mathcal{C}_{\nu,A}$ and an effective mass of $0.75m_n$ that corresponds to Figure 6. There is suppression at low $|\omega|$ s, but a resonant enhancement at high $|\omega|$ s. Note that at small $|\omega|$ s the magnitude of the correction is a strong function of position in the star and is largest at the center.

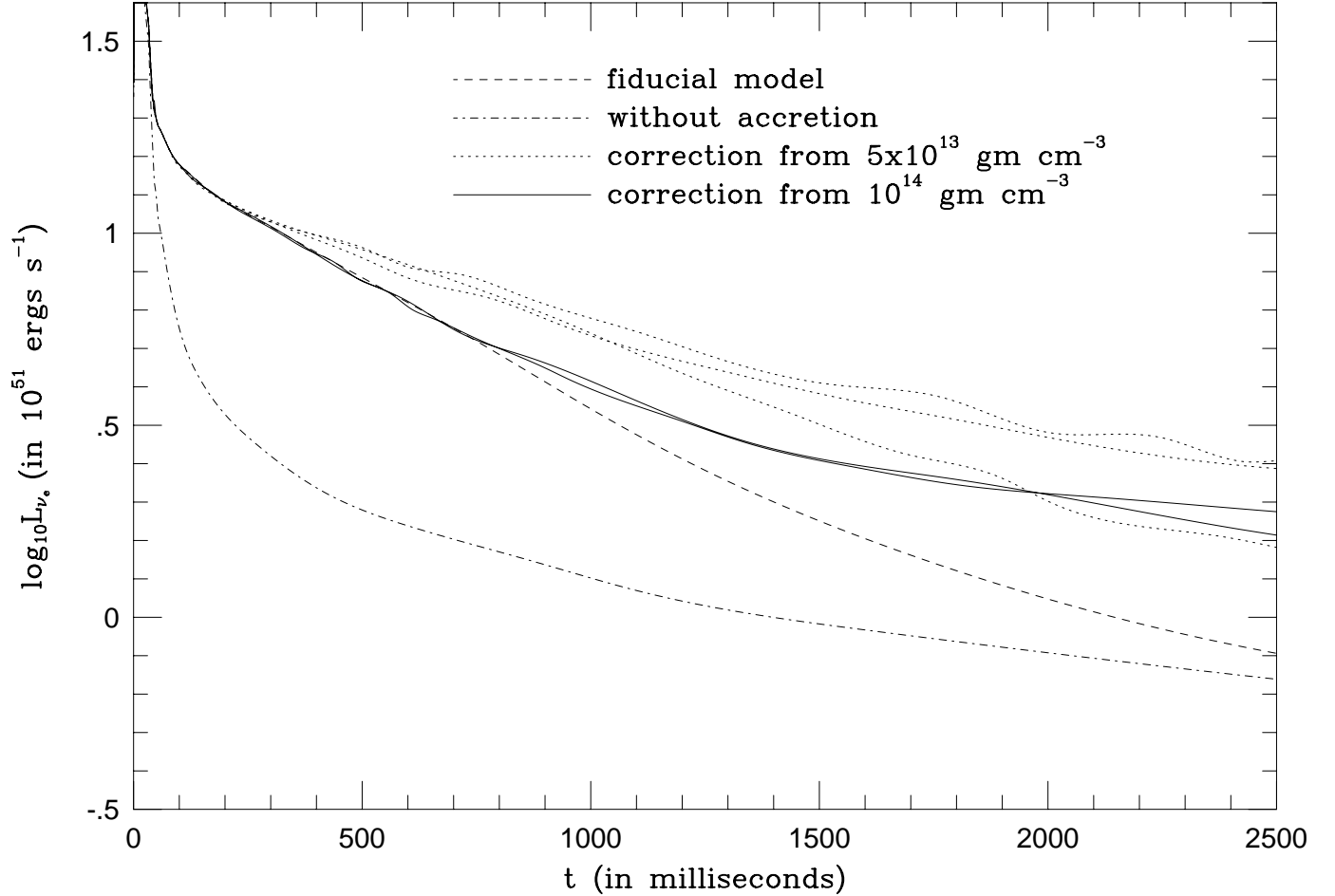


FIG. 11. \log_{10} of the electron neutrino luminosity (L_{ν_e}) in units of 10^{51} ergs s^{-1} versus time after bounce in milliseconds, with and without accretion. For the accretion models, total opacity suppression factors of 0.3, 0.1, and 0.05 were assumed above 5×10^{13} gm cm^{-3} and of 0.3 and 0.1 were assumed above 10^{14} gm cm^{-3} . The fiducial model is dashed, the model without accretion is dot-dashed, the models with correction above 5×10^{13} gm cm^{-3} are dotted, and those with correction above 10^{14} gm cm^{-3} are solid. On this plot, the models with the largest corrections have the highest luminosities after 2500 milliseconds. The comparisons between the dashed curve and all others are the most germane.